

NCAR GV Aircraft TAT Sensor Update: Signal Path Changes and Recovery Factor Modeling

Josh Carnes, NCAR Research Aviation Facility, 5/25/2022

Rev.20220603

Contents

Introduction	2
Data Observations.....	3
TAT Sensor Signal Path Summary	5
Signal Path Analysis.....	6
Recovery Factor Parameterization.....	6
Basic Theory	6
Recent Changes.....	7
Impact of Error	8
Ambient Temperature Processing Comparison.....	9
Harcos Recovery Factor Inter-Comparison.....	10
Electrical Signal Path Upgrade	12
Impact of Recovery Temperature Measurement Error	13
In-Flight Temperature Sensitivity of the Electrical Signal Path.....	13
Oil Bath Calibration	16
Engineering Calibration.....	19
Error (or Change) Analysis Summary	20
Recovery Factor Parameterization Alternate Proposal	21
Fundamental Assumptions	21
Flight Data Results	23
Parameter Optimization	25
Other Potential Areas of Concern.....	29
3-Wire Detection Circuit	29
Deicing Heat Error.....	29
Conclusions	30
Recommendations 9/2021.....	31
Appendix A: RTH1-RTH2 Pulses.....	32
Appendix B: Rosemount 102 Deiced Sensor Performance.....	34
Appendix C: Recovery Factor Estimation from Speed Runs, Derivation.....	36
References	37

Introduction

Data quality review performed during the SPICULE 2021 campaign identified discrepancies between Total Air Temperature (TAT) sensors installed aboard the NCAR Research Aviation Facility (RAF) Gulfstream-V (GV) aircraft involving, in particular, the Harco Laboratories, Inc. Model 100009-1 deiced dual-element TAT sensor and comparison to the Rosemount¹ Model 102E2AL non-deiced sensor², both shown in Figure 1. In brief, the difference between measured ambient temperatures exceeded 0.5°C in some conditions.

These observations prompted a root-cause investigation that considered recent changes to the sensor signal path and data. Three critical recent changes were identified and analyzed.

1. Modification to the recovery factor model within the ambient temperature variable derivations, updated ~8/2019, based on a 2015 analysis [1].
2. Upgrade of the sensor's electrical signal path to the newly designed "TEMP-DACQ" signal conditioner and acquisition module, installed 1/2020 as a test setup, followed by the permanent installation 1/2021.
3. Oil bath calibration of the Harco TAT sensor and calibration coefficient updates, 9/2019.

The analysis acknowledges error contributions from all changes, but focuses primarily on large systematic contributions (0.5°C) caused by the recovery factor model update. Analysis of the oil bath calibration indicates error below the level of concern (< 0.1°C). Analysis and observation of the new electrical signal path identified an intermittent error up to ~0.3C on one channel but otherwise stable performance after repair. Review of the Harco TAT sensor's recovery factor parameterization revealed a need to revisit the model. This memo summarizes the analysis and results, and proposes an update to recovery factor model parameters.



Figure 1 TAT Sensors: (a) Harco Model 100009-1 de-iced, model view, (b) Rosemount Model 102 non-deiced, actual, (c) Rosemount Model 102 de-iced, actual

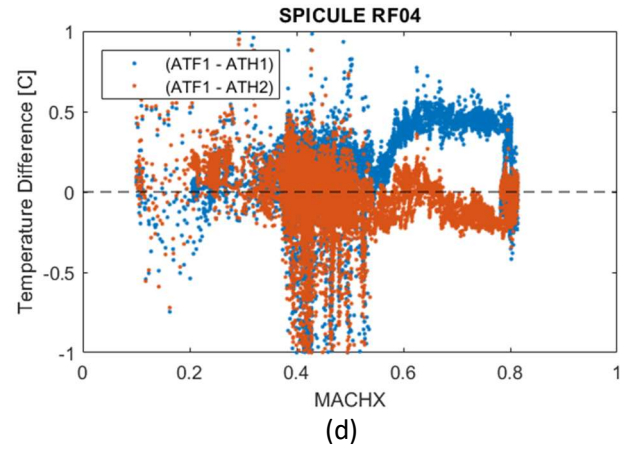
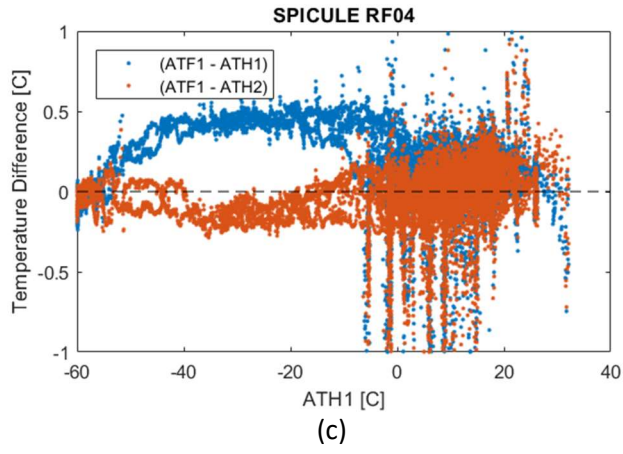
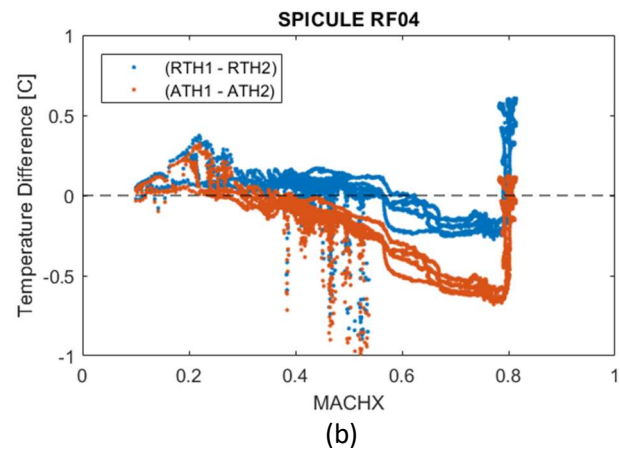
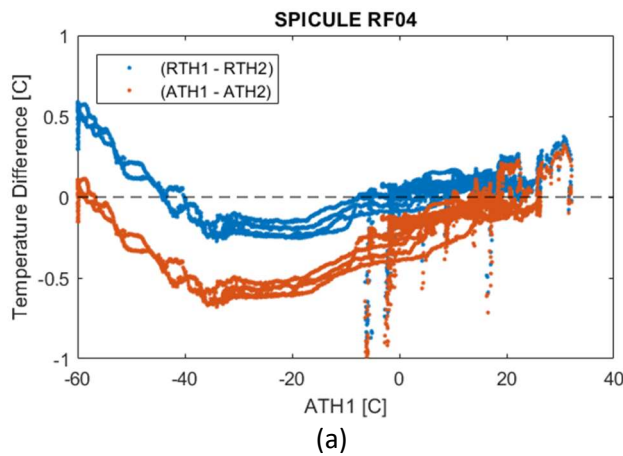
¹ Rosemount Aerospace was acquired by Goodrich Company in 1993. United Technologies Corp. (UTC) acquired Goodrich in 2011 and then Rockwell Collins in 2018 which became Collins Aerospace Systems. UTC merged with Raytheon in 2020. TAT sensors are currently managed by Collins Aerospace under this structure. The Harco TAT sensors are currently managed by HarcoSemco.

² The Harco de-iced TAT dual-element sensor signal path typically generates recovery temperature variables {RTH1} and {RTH2} and derived ambient temperatures {ATH1} and {ATH2}. The Rosemount "non-deiced, fast response" sensor generates recovery temperature {RTF1} and derived ambient temperature {ATF1}. Most campaigns over at least the last 10 years assigned {ATH1} to be the standard ambient temperature {ATX}.

Data Observations

The critical observations during SPICULE 2021 are illustrated in Figure 2(a)(b)(c)(d).³ Research flight RF04 is an example of a long flight (6 hours) that spans wide altitude and speed conditions and shows the extent of the largest sensor discrepancies. Comparison of the recovery temperature quantities $\{RTH1\}$ and $\{RTH2\}$ reveals a difference that depends on flight conditions and is amplified in the derived ambient temperature quantities $\{ATH1\}$, $\{ATH2\}$, and $\{ATF1\}$, particularly between -40 and 0°C ambient temperature and Mach > 0.6, where $\{MACHX\}$ is the standard Mach variable in the dataset. (a) and (b) show the difference between the two elements in the Harco sensor, while (c) and (d) show the differences relative to the Rosemount non-deiced sensor. (e) and (f) compare the $\{ATHx\}$ variables to the temperature measurement by the avionics system, $\{AT_A\}$. Differences are plotted with respect to measured ambient temperature $\{ATH1\}$ and to Mach, indicating some correlation with both. The full dependence is complex, with possible contributions from aircraft attitude and the aircraft's internal ambient temperature conditions that are not easily quantified. The critical observations are summarized in the following points:

- ($\text{abs}(\{ATH1\} - \{ATH2\}) > 0.5^\circ\text{C}$) at some flight conditions, particularly for ($-40 < ATH1 < 0^\circ\text{C}$), at altitudes > 9km, and Mach > 0.6.⁴
- ($\text{abs}(\{ATH1\} - \{ATH2\}) > \text{abs}(\{RTH1\} - \{RTH2\})$) in most conditions.
- ($\text{abs}(\{ATF1\} - \{ATH1\}) > \text{abs}(\{ATF1\} - \{ATH2\})$) in most conditions, indicating better matching of $\{ATF1\}$ to $\{ATH2\}$.
- ($\text{abs}(\{AT_A\} - \{ATHx\}) < 1.3^\circ\text{C}$)



³ Data had a 1Hz sample rate in the netCDF file generated 6/24/2021 with latest NIMBUS processing. Data at ($MACHX < 0.1$) and NaN values are ignored.

⁴ The large negative difference bursts between -7°C and +20°C (Mach 0.4 and 0.6) are due to in-cloud wetting and are not considered in this report.

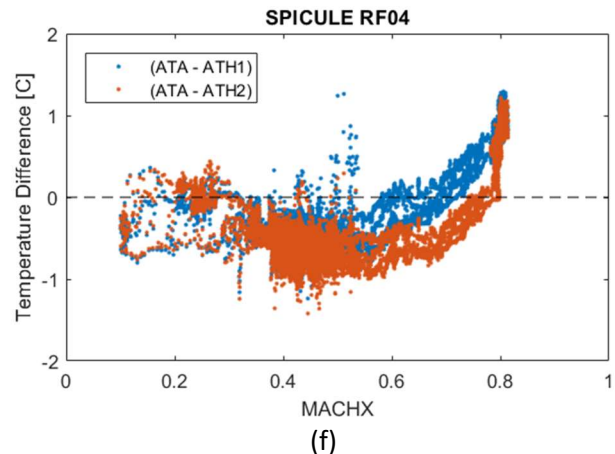
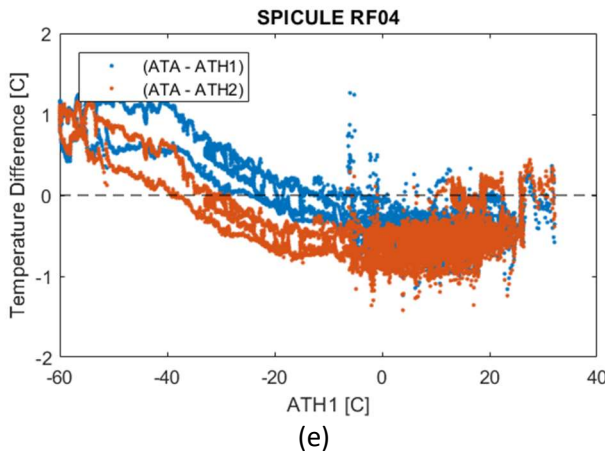


Figure 2 Temperature sensor differences exceed 0.5C during SPICULE RF04 for (a) Harco dual sensor differences vs. ATH1, (b) Harco dual sensor differences vs. MACHX, (c) difference between Rosemount non-deiced and Harco vs. ATH1, (d) difference between Rosemount non-deiced and Harco vs. MACHX, (e) difference between Rosemount non-deiced and avionics Rosemount vs. ATH1, (f) difference between Rosemount non-deiced and avionics Rosemount vs. MACHX.

Historical data shows that the critical data observations also exist in past campaigns, as observed in Figure 3 during (a) ORCAS 2016, and (b) OTREC 2019.⁵ These plots of the Harco sensor element difference vs. ambient temperature shows a similar “bow” shape with large difference error deviations at cold temperatures.

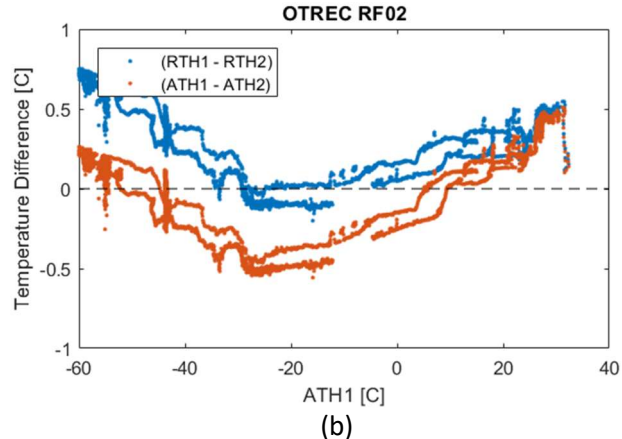
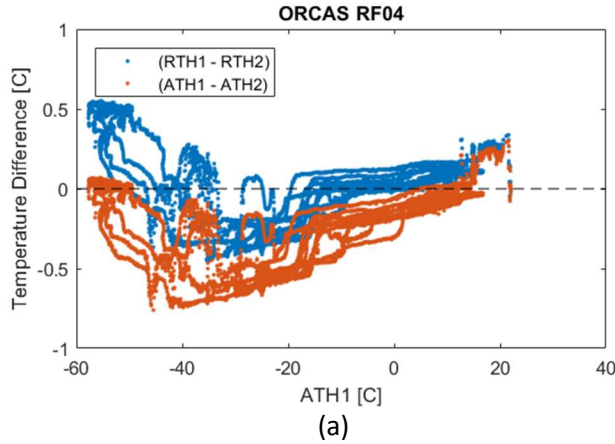


Figure 3 Temperature sensor differences also exceed 0.5C during the (a) ORCAS and (b) OTREC campaigns on the GV.

Another observation noted recently during OTREC, SPICULE, ASPIRE-TEST 2021 and MethaneAir 2021 are difference pulses: $\{\text{RTH1}\} - \{\text{RTH2}\}$ step changes followed by relaxation, occurring as a single instance or in bursts and shaped by the time response of the sensor. These occurrences are discussed in “Appendix A: RTH1-RTH2 Pulses”.

⁵ 1Hz sample rate data from netCDF files generated 4/24/2021 and 5/29/2021, respectively. Data at (MACHX < 0.1) and NaN values are removed.

TAT Sensor Signal Path Summary

The TAT sensor signal path spans physical and virtual space as shown in Figure 4, much of which is discussed in detail in [2]. The resistive elements of the TAT sensor are measured by an electrical signal conditioning and data acquisition sub-system and a measured voltage is converted to a recovery temperature $\{RTHx\}$ using conversion coefficients derived from pre-campaign calibrations. The ambient temperature $\{ATHx\}$ is then derived from Mach $\{MACHX\}$ and the (Mach-dependent) recovery factor $\{a_r\}$ per Equation 2.⁶ It is also intuitively useful to understand that the recovery temperature can be represented as the sum of the ambient temperature and a “dynamic heating” term, as described by Equation 1.

Calibration of the sensor in a temperature-controlled oil bath, commonly referred to as the “bath calibration”, characterizes the resistances of the sensor elements. Signal path calibration, referred to internally at RAF as the “engineering calibration,” inserts a resistor reference in place of the sensor elements and characterizes the static error through the wiring, signal conditioning, and data acquisition physical sub-system installed on the aircraft. By this calibration strategy, the engineering calibration coefficients correct signal path non-idealities and are not intended to correct for sensor characteristics. ADC calibration, performed at a calibration test bench in a laboratory, characterizes the offset and gain properties of the ADC device. The results from these three calibrations are combined to provide the voltage-to-temperature conversion coefficients used to calculate the recovery temperature from the measured voltage, but also compensate for the many non-ideal characteristics of the signal path, especially mean offset and gain errors.

The ideal conversions are given in Table 1.

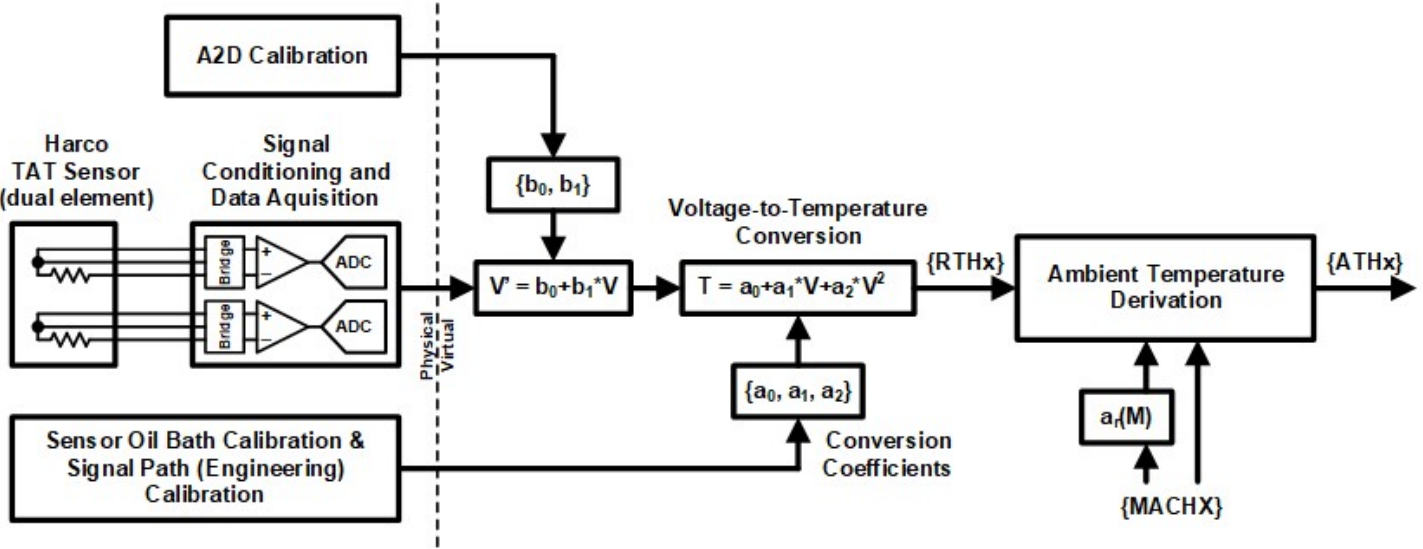


Figure 4 TAT sensor signal path block diagram.

$$\{RTHx\} = \{ATHx\} + Q(\{MACHX\}, \{a_r\}, \{ATHx\})$$

Equation 1 Recovery temperature representation of the sum of ambient temperature and dynamic heating.

$$\{ATHx\} = \frac{\{RTHx\} + T_0}{\left(1 + a_r \cdot \{MACHX\}^2 \cdot \frac{R'}{2c_v}\right)} - T_0$$

Equation 2 Ambient temperature derived from the recovery temperature, Mach, and recovery factor.

⁶ Recovery temperature is sampled at 100Hz and then sub-sampled (with filtering) to 25Hz or 1Hz for calculation of the ambient temperature. Additional information about the ambient temperature derivation, including full details for the equation, is available in the RAF Processing Algorithms document [10].

Table 1 Temperature signal path ideal conversions, assuming the ideal CVD model and the Temperature Amplifier circuit gain

Conversion	Ideal Equation	2 nd Order Polynomial Fit
Temperature-to-Resistance	CVD R(T) Model See Ref. [3]	$R'(T) = 50.00 + 0.1991*T - 3.003e-5*T^2$, See Footnote ⁷
Resistance-to-Voltage	$V(R) = 125*(R / (R+500) - 34/534)$ See Footnote ⁸	$V'(R) = -78.67 + 0.2442*R - 3.758e-4*R^2$, See Footnote ⁹ $R'(V) = 34.01 + 4.551*V + 0.04257*V^2$, See Footnote ¹⁰
Voltage-to-Temperature	-	$T'(V) = a_0 + a_1*V + a_2*V^2$ $T'(V) = -79.28 + 22.25*V + 0.3029 * V^2$, See Footnote ¹¹ $V'(T) = 3.405 + 0.04115*T - 2.110e-5*T^2$, See Footnote ¹²

Signal Path Analysis

In-flight measurements and in-lab characterization data was analyzed to quantify the impact of the recent signal path changes and identify contributions to the observed differences between sensors. A comprehensive analysis of the signal path is also described in [2], which focused on the critical issues in 2014. In-flight verification of the signal path stability was also performed during a test flight and the ASPIRE'21 campaign.

Recovery Factor Parameterization

Basic Theory

The recovery factor of a sensor quantifies the portion (< 1) of kinetic energy that is successfully transferred to heat as the incoming airflow is slowed (relative to the aircraft frame of reference) before reaching the sensor element. The air sensed at the element is above the ambient temperature, typically 10-30C during typical GV flight conditions, by this “dynamic heating.”

The TAT recovery factor model used in the ambient temperature derivation depends on Mach, a dependence identified at RAF as significant around 2012 and reported in [2]. Processing prior to this time assumed a constant recovery factor. The Harco Model 100009-1 sensor is similar in design to the industry standard Rosemount Model 102 deiced (heated, configuration -a) sensor, and therefore its response is assumed to be similar. The recovery factor of the Rosemount version (Figure 5) was characterized in wind-tunnel experiments and well documented in the Rosemount/Goodrich “Total Temperature Sensors Technical Report 5575,” [4] allowing precise modeling of the Mach speed dependence. The Harco sensor has no such documented characterization, but its mechanical drawing [5] specifies “RECOVERY ERROR: LESS THAN 0.5% OF THE TRUE TAT (IN KELVIN) AT MACH 1.0.” Assuming that “RECOVERY ERROR” is equivalent to the “Recovery Correction” described in [4], the 0.5% recovery error is equivalent to a recovery factor of 0.97 at Mach 1.0. This limited description of the Harco recovery error may result in up to 0.03 (~3%) recovery factor error that translates to an ambient temperature error of 0.7 to 0.9°C at Mach 0.8, a typical cruising speed of the GV. Previous efforts at RAF have attempted to characterize the Harco sensor recovery factor more accurately across Mach conditions [1].

⁷ $R'(T)$ is a 2nd order polynomial fit to the Ideal CVD model given in [3].

⁸ $V(R)$ is the ideal voltage transfer function of the electrical amplifier circuit that measures resistance and output voltage.

⁹ $V'(R)$ is a 2nd order polynomial fit to the Ideal Equation provided.

¹⁰ $R'(V)$ is an inverted 2nd order polynomial fit to the Ideal Equation provided.

¹¹ $T'(V)$ is an inverted 2nd order polynomial fit to $V(R=R'(T))$, where the coefficients correspond to those in Figure 4.

¹² $V'(T)$ is a 2nd order polynomial fit to $V(R=R'(T))$

FIGURE 14
WIND TUNNEL DATA; MODEL 102 RECOVERY CORRECTIONS

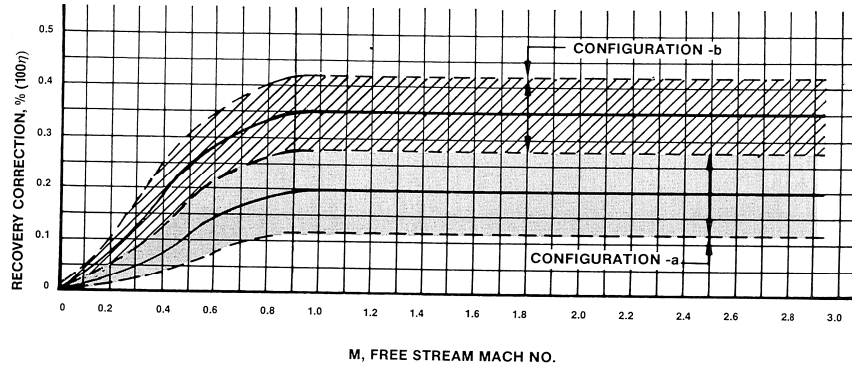


Figure 5 Recovery correction wind-tunnel characterization curve for the Rosemount 102 de-iced sensor (configuration-a) from [4].

Recent Changes

Following the analysis of [1], the recovery factor parameters of the TAT sensors were changed in the NIMBUS data processing software around 8/2019. At the time of the change, all TAT sensors had been modeled in the form of Equation 3, where 'M' is the Mach speed and represented by the {MACHX} measurement.¹³ Table 2 shows how the parameter values were changed and Figure 6 shows the changes to the Harco sensor recovery factor model.

$$a_r(M) = C0 + C1 \cdot (\log_{10} M) + C2 \cdot (\log_{10} M)^2 + C3 \cdot (\log_{10} M)^3$$

Equation 3 Recovery factor parameterized model for TAT sensors.

Table 2 Changes to the TAT sensor recovery factor model parameter values.

Sensor	C0	C1	C2	C3
Pre-8/2019				
Harco 100009-1 de-iced, element 1 & 2	0.988	0.053	0.090	0.091
Rosemount 102 de-iced, elements 1 & 2	0.988	0.053	0.090	0.091
Rosemount 102 non-deiced, element 1	0.9959	0.0283	0.0374	0.0762
Post-8/2019				
Harco 100009-1 de-iced, element 1	0.986	No Change		
Harco 100009-1 de-iced, element 2	0.969	No Change		
Rosemount 102 de-iced, elements 1 & 2	0.958	No Change		
Rosemount 102 non-deiced, element 1	No Change			

¹³ This author assumes that the recovery factor model was chosen initially to fit the recovery factor data presented in Figure 5 which appears to converge to zero recovery correction at Mach 0. The recovery factor model is nearly linear from Mach 0.3 to 1.0 but strongly decreases for Mach < 0.2, a feature that de-emphasizes thermal recovery compensation but is not clearly supported by the data due to the ambiguity in the conversion from zero recovery correction to recovery factor. The reasoning behind selection of this model over a simple linear model is unknown to scientists at RAF at this time, although it is thought to have minimal effect on data because speeds below 0.2 Mach are rarely encountered. Evidence for a physical basis for reduced recovery factor at low Mach has not been found by this author.

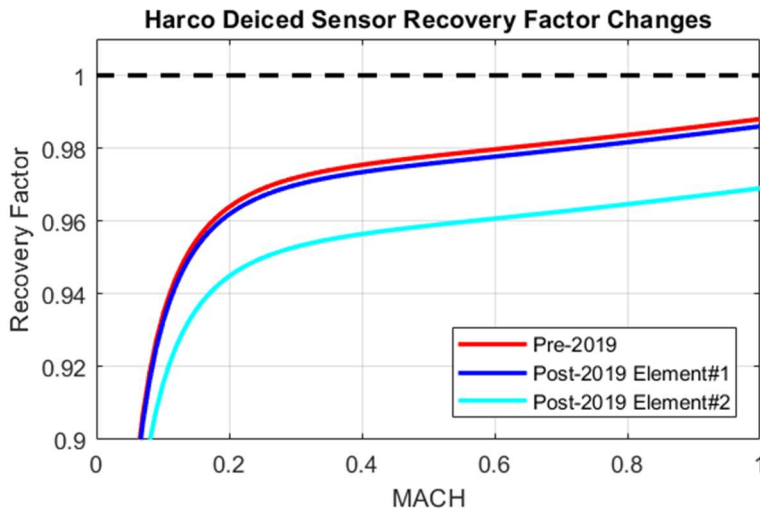


Figure 6 Recent changes to the Harco deiced sensor recovery factor model curves.

Impact of Error

The impact of a recovery factor error varies at different flight speeds and ambient temperatures due to the amount of dynamic heating that must be compensated. To understand the magnitude of the impact, a simple model of the correlation between Mach speed and ambient temperature during typical flight conditions for the GV is assumed, described here and shown in Figure 7.¹⁴

- Mach 0.8, typically the fastest speed reached in flight, occurs at altitudes corresponding to $< -40^{\circ}\text{C}$.
- Between -40 and $\sim 0^{\circ}\text{C}$, the Mach speed typically has a linear relationship with slope of $-0.0075 \text{ [C}^{-1}]$. This typical linear relationship is due to the ram pressure limit of the aircraft in the 4km to 9km altitude region.
- Mach < 0.3 is only during take-off and landing, with near-constant relationship at the ground temperature.

Assuming a recovery factor similar to the Rosemount 102 deiced sensor data given in [4] and the typical GV flight conditions model defined here, the amount of dynamic heating and error due to the recovery factor is shown in Figure 8.¹⁵

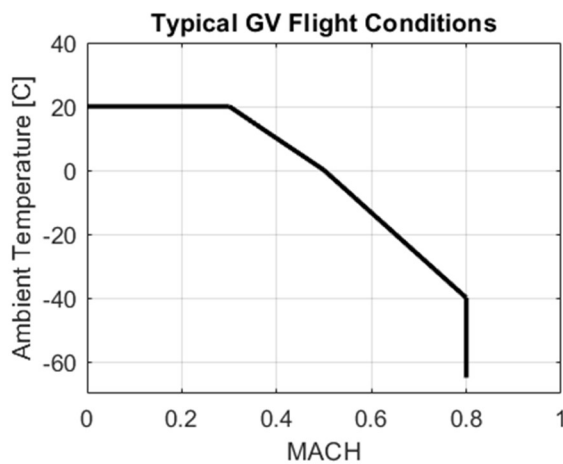


Figure 7 Simple Mach vs. ambient temperature model for the GV during typical flight conditions.

¹⁴ The general correlation between Mach and ambient temperature can be viewed during any campaign with the GV, with variations depending on season, location, and how science objectives impact flight plans. See SPICULE, OTREC, SOCRATES, CSET, etc.

¹⁵ As a comparison, the C-130 airspeeds are typically between Mach 0.3 and 0.45, altitude $< 7.6\text{km}$, and ambient temperatures $> -40^{\circ}\text{C}$. At these slower speeds, the dynamic heating correction is limited to $\sim 12^{\circ}\text{C}$. Therefore, dynamic heating errors are $\sim 3x$ smaller than for the GV.

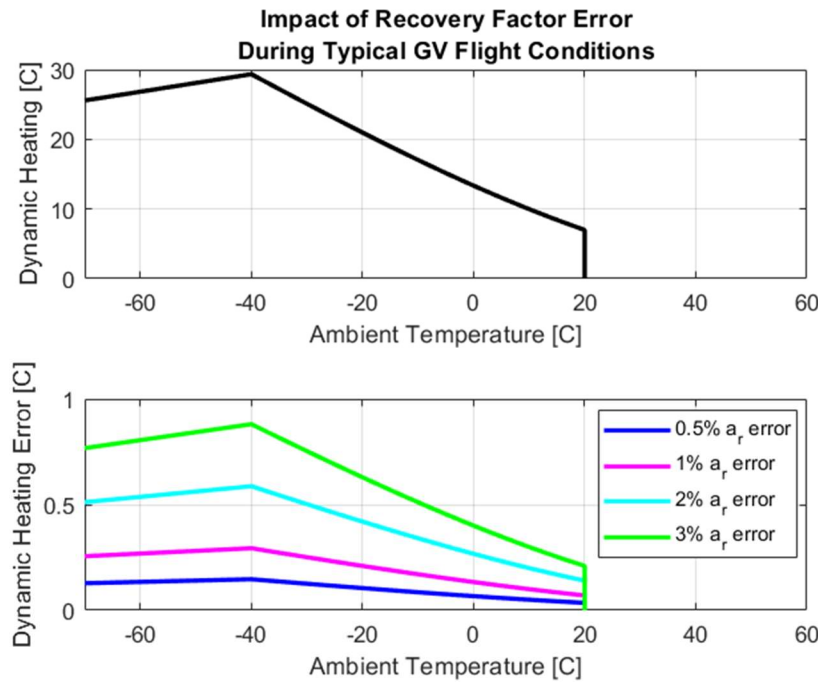


Figure 8 Approximate impact of recovery factor error during typical GV flight conditions.

Given the limited information provided with the Harco sensor by the vendor, a 2% recovery factor error is very possible, and the resulting dynamic heating compensation error ($> 0.5^{\circ}\text{C}$) is motivation to perform recovery factor characterization to reduce the error to $< 0.5\%$, if possible. Conversely, a biased characterization of a_r may permanently embed an error into the post-processing. The recent 8/2019 post-processing updates to the Harco recovery factor model shifted the element #1 {RTH1} recovery factor by only 0.02%, but the element #2 {RTH2} recovery factor was changed by 1.9%. Additionally, the C0 parameter for the Rosemount model 102 deiced sensor recovery factor model was changed by 3%.

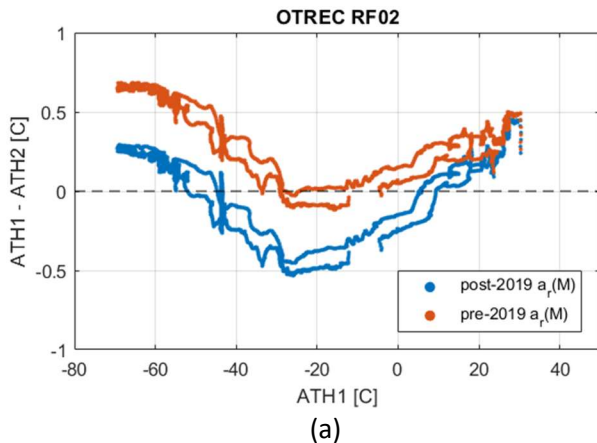
Ambient Temperature Processing Comparison

The recovery factor parameter update of 2019 had a clear impact on the difference observed between the two ambient temperatures measured from the Harco sensor. Campaigns such as OTREC 2018, ECLIPSE 2019, and MethaneAir 2021 have small ($\{\text{ATH1}\} - \{\text{ATH2}\}$) difference for the majority of the time because most flight time is spent at very high altitudes and cold temperatures where the matching is good with the post-2019 parameters. Performance at mid-altitudes, visited often during SPICULE 2021, exceed 0.5°C and raise concern.

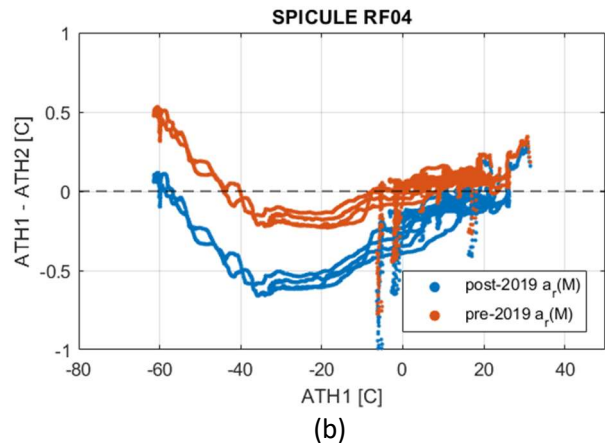
Figure 9 shows the ($\{\text{ATH1}\} - \{\text{ATH2}\}$) difference vs. $\{\text{ATH1}\}$ for the Harco de-iced sensor during (a) OTREC RF02 and (b) SPICULE RF04 using the pre-2019 and post-2019 processing. The figures both demonstrate how the changes to the recovery factor C0 parameter tilts the difference curves, making the high altitude difference smaller at the expense of mid-altitude values. Changing the C0 coefficients does not impact the non-linearity (or multi-variable dependence) of the difference, so tuning C0 cannot reduce the difference to less than $+/-0.4^{\circ}\text{C}$ over those flight conditions.

Applying the processing further into the past suggests that performance varies among sensor units. Whereas OTREC and SPICULE used Harco S/N#630393, DEEPWAVE and CONTRAST in 2014 used S/N#812452¹⁶. Figure 10 demonstrates good matching to low temperatures for this sensor unit using the pre-2019 recovery factor, although #812452 also shows a large deviation starting at -55°C .

¹⁶ Harco S/N#812452 was installed during CONTRAST as {RTH3} and {RTH4}, whereas DEEPWAVE installed as {RTHR1} and {RTHR2}.

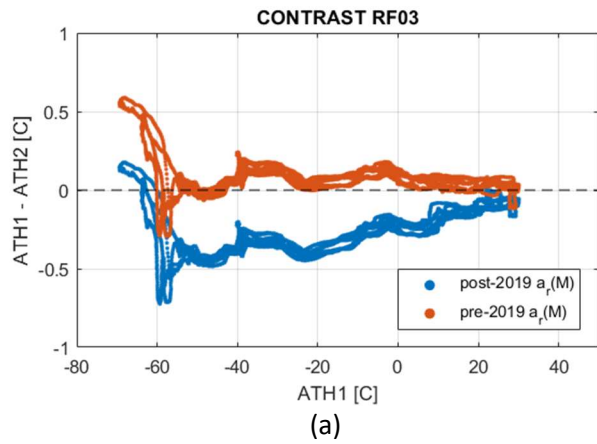


(a)

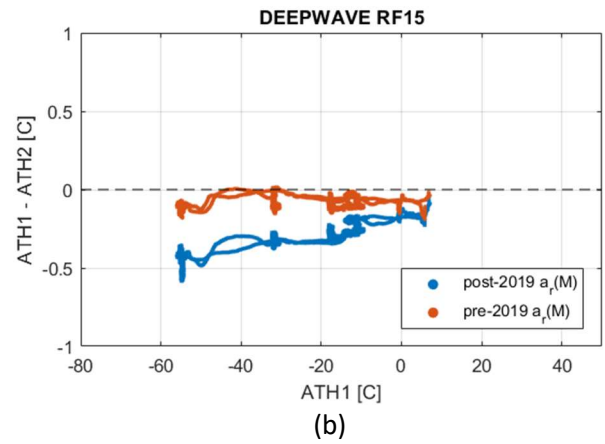


(b)

Figure 9 Ambient temperature difference between the Harco Elements for (a) OTREC RF02 and (b) SPICULE RF04 with pre- and post-2019 processing.



(a)



(b)

Figure 10 Ambient temperature difference between the Harco S/N#812452 elements for (a) CONTRAST RF03 and (b) DEEPWAVE RF15.

Harco Recovery Factor Inter-Comparison

Accurately characterizing the recovery factor of a sensor and applying that characterization across many sensors assumes that all sensors respond similarly. The recovery factor variation between Harco sensor elements and the validity of applying one characterization across many elements may be estimated by observing the difference between two elements in one sensor head, and is readily estimated from available campaign data. This technique assumes that the difference between elements is entirely due to recovery factor variation, which is not necessarily true. The technique also does not necessarily describe variation from one Harco sensor head to the next, rather, it is a proxy estimate.

The derivation begins by expressing the recovery temperature as a sum of ambient temperature and dynamic heating, and then calculates a difference between two sensor's recovery temperatures (sampling the same air) from which the recovery factor difference is found in the simple and intuitive form of Equation 4.

$$(T_{r1} - T_{r2}) = \underbrace{(T_{a1} - T_{a2})}_0 + (\alpha_{r1} - \alpha_{r2})T_a M^2 R' / 2c'_v \xrightarrow{\text{yields}} \alpha_{r1} - \alpha_{r2} = \frac{2c'_v}{R'} \cdot \frac{T_{r1} - T_{r2}}{T_a M^2}$$

Equation 4 Recovery factor difference comparison.

This comparison generally cancels signal path electronics temperature drift and some systematic calibration errors in the recovery temperature terms, and an ambient temperature estimate (T_a) error of < 1C results in a difference calculation error < 0.5%, therefore it gives an accurate description of the recovery factor difference variation. The effects of moisture on the $\frac{2c'_v}{R'}$ term are also limited to a change of < 1%¹⁷, which is also not significant for this calculation when

¹⁷ This is a conclusion from the "Moist-air Considerations" of [10], and a "worst-case" assumption of saturated vapor pressure of $e \sim 24\text{hPa}$ at 20C and 600hPa ambient pressure, resulting in vapor pressure always < 4% of atmospheric pressure.

compared to other sources of variation apparent in the data. Calibration inaccuracy and signal path measurement errors affect this analysis and are limitations of using flight data to characterize the recovery factor, in general.

Data from three different Harco sensor heads are analyzed here across the following campaigns, with detailed tracking to maintain correct assignment of the two sensor elements to the {RTH1} and {RTH2} variables to preserve the difference polarity. Recovery factor difference data is binned according to Mach value and each flight is bin averaged.

- S/N#630393 (SPICULE'21, SOCRATES'18, ORCAS'16, CSET'15, 23 flights total)
- S/N#812452 (ACCLIP-TEST'20, DEEPWAVE'14, IDEAS-IV'13, 11 flights total)
- S/N#708094 (DC3'12, TORERO'12, 9 flights total)

The results of Figure 11 show that variations between elements in the same head have recovery factor difference of typically less than 0.015, or roughly 1.5% recovery factor error as it relates to Figure 8, and that element #1 is not significantly offset from element #2 in a mean sense over the whole Mach range. The general trends of S/N#630393 and S/N#708094 demonstrate element difference that varies enough from one sensor head to the next such that any attempt to correct for differences between elements would not apply to a different sensor head. Results from S/N#812452 show a division gap between the campaigns analyzed (with DEEPWAVE being offset from others), likely due to differences in signal path calibration between campaigns. Additionally, the unique trend of S/N#630393 and its strong divergence near Mach 0.8 are notably different than the other two sensors heads. This analysis suggests that, based on the performance history of operating these sensors, characterizing the recovery factor with historical flight data and applying a fitted characterization model to all sensor elements would likely have recovery factor error of approximately +/-1.5% across the Mach range. Similarly, using the same recovery factor parameters for both elements of a sensor head based on an average of the characterization of each element would result in 0.75-1.5% recovery factor error across the Mach range. This element-to-element variation is of similar magnitude to the error imposed by the lack of information about the Harco sensor, therefore, the strategy of characterizing the recovery factor with flight data and applying the characterized model across all sensor heads may not result in the desired error reduction when compared to the pre-2019 model.

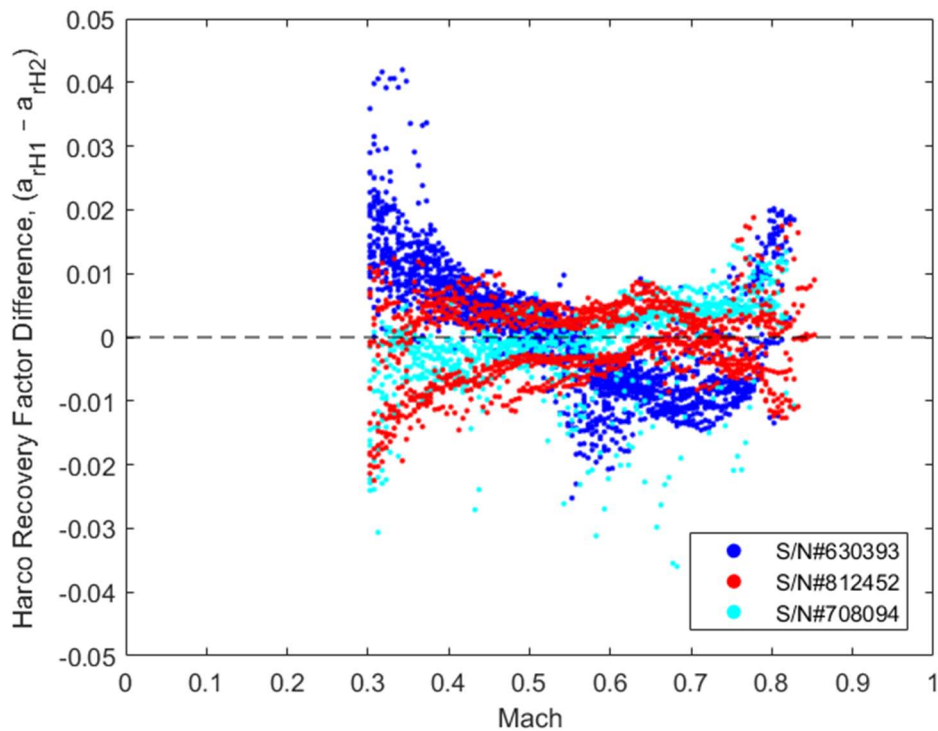


Figure 11 Recovery factor difference between sensor elements for a few Harco sensor units.

Electrical Signal Path Upgrade

The electrical signal paths of the sensor channels in the GV were modified in January 2020. The “Temperature Amplifier” modules (located in the GV Radome Environmental Box, shown as the “Bridge” and Operational Amplifier of Figure 4) and the NCAR ADC digitization card were removed from the signal path and replaced with two custom “TEMP-DACQ Integrated Modules” that each provide two sensor channels. The TEMP-DACQ Integrated Module combines two “Modified Temperature Amplifiers” and a TEMP-DACQ printed circuit board. Together, the circuits condition, amplify, and digitize the resistivity measurement of the sensor element, and compose the entire signal conditioning and data acquisition block of Figure 4. The design is further documented in [6] and [7], and the unit conversions through the signal path are ideally expressed with the equations of Table 1.

The TEMP-DACQ Integrated Module addressed key performance limitations of the previous solution [2] [8]. Table 3 shows the dominant errors of the previous solution compared to the new solution, where the errors are typical values translated to measured recovery temperature error.¹⁸ Temperature-dependent errors in the table are relative to the environmental conditions inside the GV radome. Introduction of the TEMP-DACQ modules significantly reduced the gain and offset temperature dependence and improved the noise performance.

Table 3 also includes error contributions from the Temperature Amplifier voltage reference, and sensor interconnect cabling which remain uncompensated. Note that the sensor interconnect cabling temperature dependence error has always been significant (up to 0.3°C over a 60C radome temperature range) and will always remain a limitation of the 3-wire detection circuit utilized.¹⁹ In summary, the table shows that the largest remaining electrical signal path errors are the TempAmp Gain Temperature dependence, and the Sensor Interconnect Temperature dependence.

Table 3 Typical errors in the temperature channel electrical signal path for the TEMP-DACQ integration module vs. the previous solution composed of the NCAR TempAmp and NCAR ADC digitizer card.

Error Type ²⁰	TempAmp + NCAR ADC	TEMP-DACQ Integrated Module	Note
Offset, Static, Pre-Calibration	5 °C	0.013 °C	Dominated by ADC offset. Error is reduced by ADC and Engineering calibration.
Offset, Temperature Dependence	0.013 °C/°C	0.000050 °C/°C	Dominated by TempAmp LT1010. Regularly experienced ~30°C ambient temperature range. LT1010 removed from TEMP-DACQ Module.
ADC Gain ²¹ , Temperature Dependence, Pre-calibration	0.030 °C/°C	0.00034 °C/°C	NCAR ADC error reduced by calibration [8]. Regularly experienced ~30°C temperature range.
ADC Noise	0.0025 °C-rms	0.00018 °C-rms	100Hz sample rate
TempAmp Gain, Temperature Dependence		0.004 °C/°C	Dominated by TempAmp AD589. Regularly experiences 20°C ambient temperature range.
Sensor interconnect cabling Temperature Dependence		0.005 °C/°C	Temperature dependence of ~10ft. copper cable. Regularly experiences 40 to 50°C temperature range.
Calibration Cable		-0.13°C	Due to length of calibration cable, ~30mΩ. Compensated during engineering calibration. ²²

¹⁸ Throughout this document, estimates of error assume an approximate relationship in the signal path between measured temperature, sensor resistance, and signal voltage such that 0.1 °C ~ 20mΩ ~ 4mV based on the sensor characteristics and Temperature Amplifier gain.

¹⁹ 3-wire RTD circuits are often capable of calibration that estimates the impact of interconnect cable resistance, but the complexity of the calibration and required hardware features has prevented feasible implementation within the GV radome installation.

²⁰ All quantities are typical and were measured by device characterization or found in individual component datasheet specifications.

²¹ Reported gain error temperature dependence assumes ~4.5V signal at the ADC input, corresponding to about 28C.

²² Engineer calibration compensates for the cable from within the AEROS calibration utility, which subtracts from the resistance set points. The 30mΩ resistance value is hard-coded in the AEROS source code.

Impact of Recovery Temperature Measurement Error

Signal path error results in error of the recovery temperature measurement, and it is important to understand how a recovery temperature (RT) error translates to an ambient temperature (AT) error. By adding simulated measurement error to Equation 2, and assuming the “Pre-2019 Rosemount 102 de-iced” recovery factor model of Table 2, results in the heat map plot of Figure 12 that shows that the ratio of AT error to RT error is generally between 0.9 to 1.0. Therefore, as a rule of thumb approximation, error in the recovery temperature measurement impacts the derived ambient temperature by about the same amount.

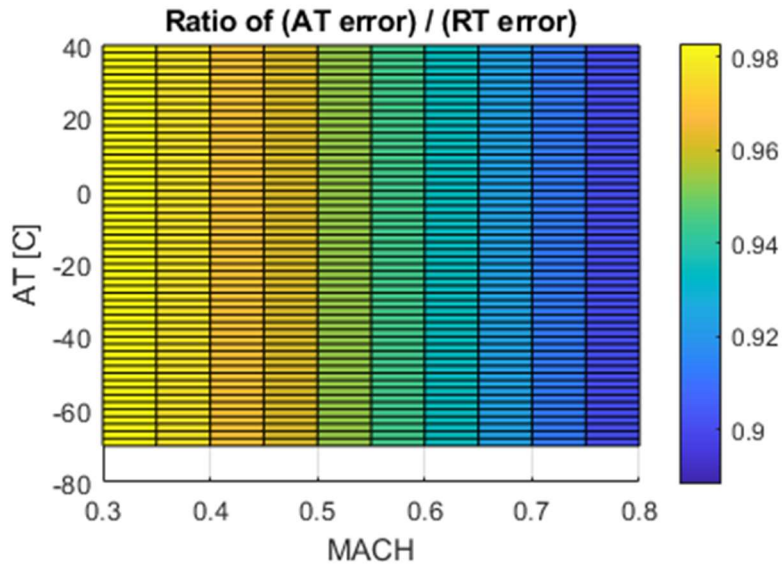


Figure 12 Ratio of Ambient Temperature error to Recovery Temperature measurement error.

In-Flight Temperature Sensitivity of the Electrical Signal Path

Precision, fixed resistor reference terminations²³ were created for in-flight characterization of the signal path stability and were demonstrated during the 11/2/2021 GV test flight, with the installation shown in Figure 13. The terminations directly substituted a 2-element TAT probe on the right-side location, variables {RTH1} and {RTH2}, and a 1-element TAT probe on the left-side location, {RTH3}. The 50Ω terminations on each channel were equivalent to a 0°C measurement from the TAT probes, although engineering calibrations were not performed to achieve an optimal mean value, so a slight offset existed. Data was collected during the flight to quantify the change in each channel measurement as the temperature conditions in the GV radome and wheel well changed during flight. Errors are reported here in the equivalent measured temperature units.

²³ The reference terminations, based on Vishay Y145350R0000T9L resistors mounted in a MS-connector’s extended back-shell, were characterized in a temperature chamber to have $< 0.01 \text{ m}\Omega/\text{ }^\circ\text{C}$ error.

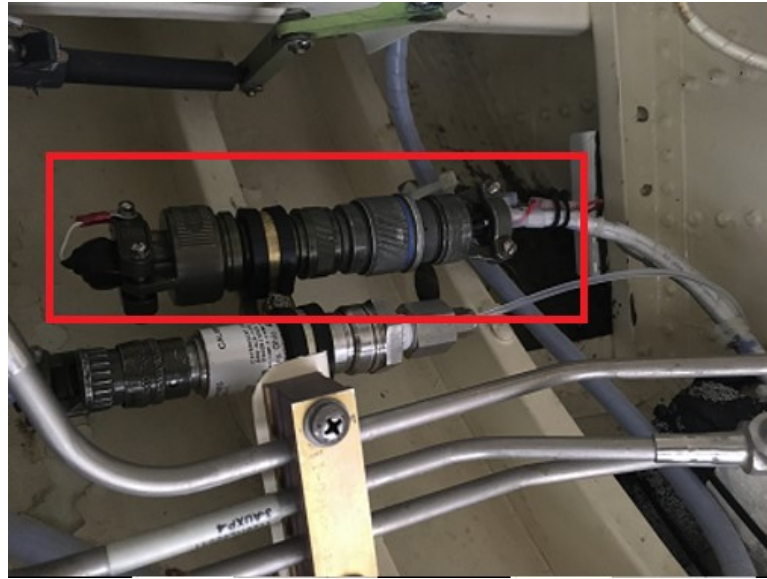
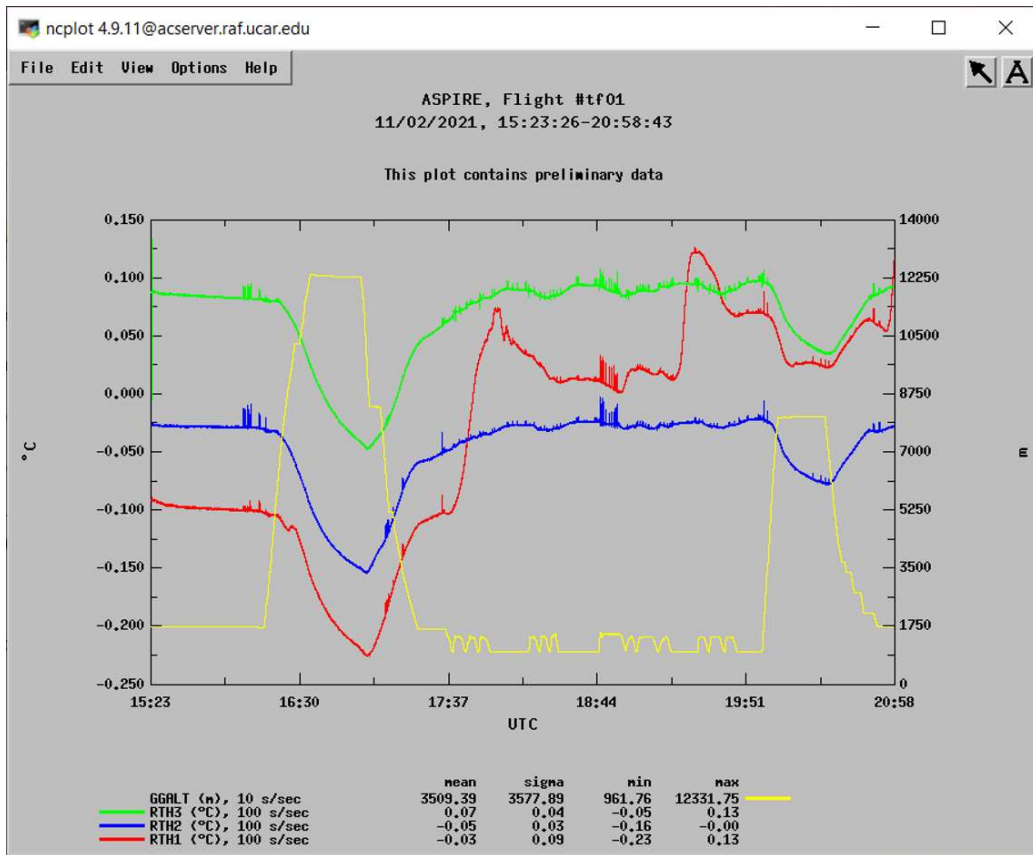


Figure 13 Installation of the dual-channel resistor reference termination in the right-side TAT channels inside the GV wheel well

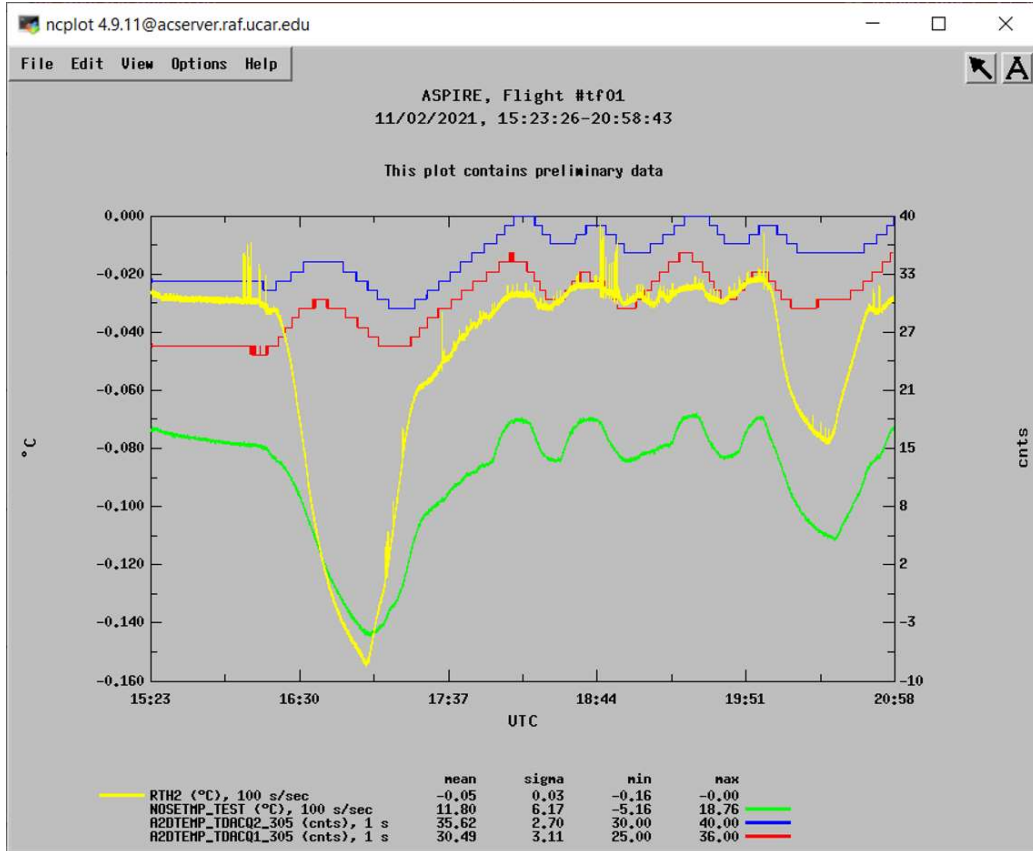
The test flight was composed of out-and-back ferry segments with near-ground maneuvers in between. The measured radome cavity temperature, {NOSETMP}, decreased 21°C during the out-bound 45-minute ferry segment while the external ambient temperature was -61°C. The TEMP-DACQ modules varied by 9°C. All channels had higher correlation with the radome air temperature than with the TEMP-DACQ module temperature, as evident during the out-bound segment when heater activation caused the TEMP-DACQ modules to initially increase in temperature instead of decrease. Channels {RTH2} and {RTH3}, representing two entirely different signal paths on different sides of the aircraft, tracked with <0.03C difference variation across the whole flight and each had 0.0065°C/C error dependence relative to the radome air temperature, as shown in Figure 14(a). This measurement agrees with the expected error due to the “Sensor Interconnect Cabling” error (0.005°C/C) supplemented by the “TempAmp Gain” error (0.004°C/C), as described in Table 3. In theory, the error is dominated by the former because the cables are exposed to a wider temperature range, and the higher amount of correlation with the radome temperature observed in the measurement of Figure 14(b) confirms the expectation.

The {RTH1} channel tracked the other channels during much of the flight, but had a ~0.2°C cumulative positive shift over time, most of which occurred rapidly at specific moments, as evident in the red curve of Figure 14(a). After the flight, TEMP-DACQ S/N#5 was removed from the aircraft and the root-cause was found to be sensitivity of an internal interconnect pin resistance to temperature/mechanical stress on this channel. The TEMP-DACQ #5 wiring was modified to eliminate the offending pin interconnect from the module signal path, reduction of the sensitivity was verified in a temperature chamber, and the module was re-installed in the GV for operation prior to the ASPIRE campaign. The design modification is recommended for all other TEMP-DACQ units, as well.

Another notable observation from the test flight is error pulses of +0.01 to +0.02°C amplitude that occurred sporadically throughout the flight, but more commonly at the lower altitudes, for example in Figure 13(a) at 18:44. The pulses occurred simultaneously across all three measurement channels, lasted 3 to 6s, and appeared to be amplitude modulated. Similar pulses are not apparent in data from recent campaigns (SPICULE, ASPIRE-TEST, MethaneAir'21) and have different properties than those described in “Appendix A: RTH1-RTH2 Pulses”. The root-cause remains unknown but is suspected to be related to system grounding, cable shielding, and/or noise coupling from adjacent cable infrastructure.



(a)



(b)

Figure 14 (a) Measurements of RTH1, RTH2, and RTH3 during the 11/2/2021 test flight using fixed resistor reference terminations. (b) Error drift showed higher correlation with GV radome air temperature (NOSETMP_TEST) than with the TEMP-DACQ module temperature (A2DTEMP_TDHCQx_305)

The ASPIRE'2021 campaign followed shortly after the test flight, allowing additional data to be collected with the dual resistor reference installed on the left-side location on variables {RTH3} and {RTH4} for long durations at cold ambient temperatures. The data from RF01 through RF03 confirmed the $\sim 0.006^\circ\text{C}/^\circ\text{C}$ signal path error dependence on the radome ambient temperature. The total deviation from the expected, constant value on these channels remained below 0.21°C for all flight time.

Oil Bath Calibration

All TAT sensors used by the RAF undergo oil bath calibration to determine the temperature vs. resistance relationship. Work by Cooper and Friesen in 2010-2014 [2] [9] identified temperature accuracy issues with the RAF calibration oil bath applied to campaigns such as PREDICT'2010, after which RAF employed a higher quality oil bath calibration performed by the NCAR EOL In-Situ Sensing Facility (ISF) [2].

Calibration of the Harco sensor S/N#630393 was performed in 3/2013, 7/2016, and 12/2019 with good consistency. Bath calibration data files are composed of measurements from -60 to $+30^\circ\text{C}$ (or $+40^\circ\text{C}$), in steps of 10°C , with 20 or more measurement points per temperature set point. The resistance versus temperature results are imported into the RAF Calibration Editor utility (caledit, deployed ~ 2011), which averages the results for each temperature set-point and generates coefficients for a 2nd order polynomial fit.²⁴ The averaged results and fit coefficients are then stored in the RAF calibration database to be used during Engineering Calibration and data processing. Comparison here is performed using the 2nd order polynomial fit curves and the results are compared to the *ideal* MIL-P-27723E Callendar – Van Dusen (CVD) curve (and the limits) defined in [3].

Figure 15 shows the resistance difference between the bath calibration results and the ideal CVD curve for Harco S/N#630393 element #1, as well as the CVD limits. The variation of calibration results from the three different dates is less than 0.008Ω (corresponding to $\sim 0.04^\circ\text{C}$) across the full temperature range. The results from element #2 are similar, as shown in Figure 16. The difference between elements #1 and #2 at each calibration date is shown in Figure 17. The notable polarity inversion during the 2016 calibration, and the comparisons to the ideal CVD curve strongly suggest that the element #1 and #2 were swapped during the 2016 calibration, resulting in additional error up to 0.008Ω ($\sim 0.04^\circ\text{C}$) between 2016 and 2019. Overall, the bath calibration consistency is good relative to observed measurement discrepancies outlined in “Data Observations”.

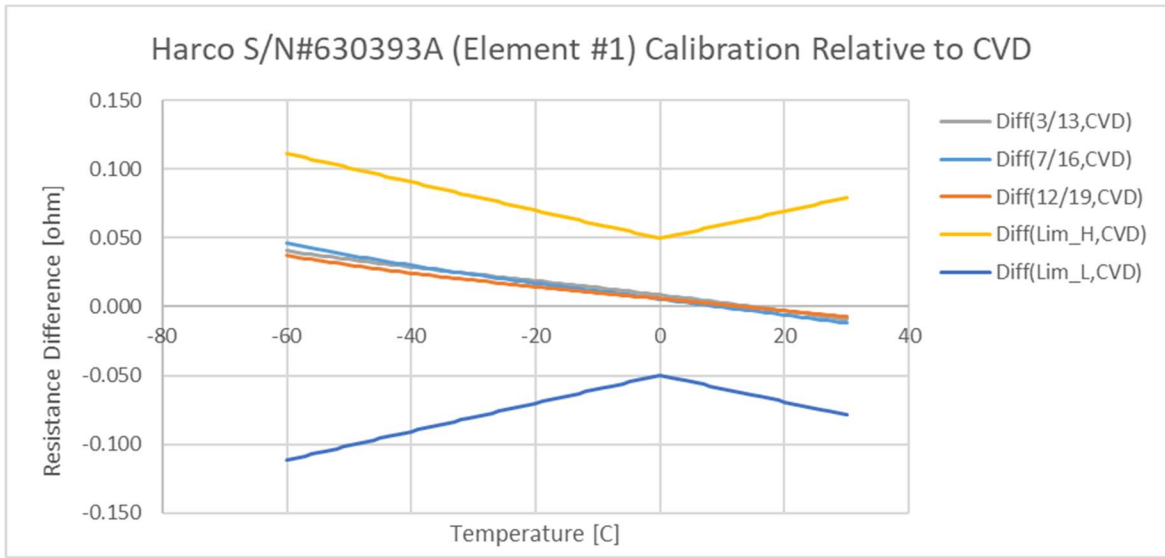


Figure 15 Harco element #1 calibrations relative to the ideal CVD curve and including limits per MIL-P-27723E.

²⁴ Data are not currently fitted to the Callendar – Van Dusen equation of MIL-P-27723E in the calibration procedure as prescribed in [2]. A 2nd order polynomial fit matches the equation to within $1.5\text{m}\Omega$ ($\sim 0.007^\circ\text{C}$) which is sufficient for this application.

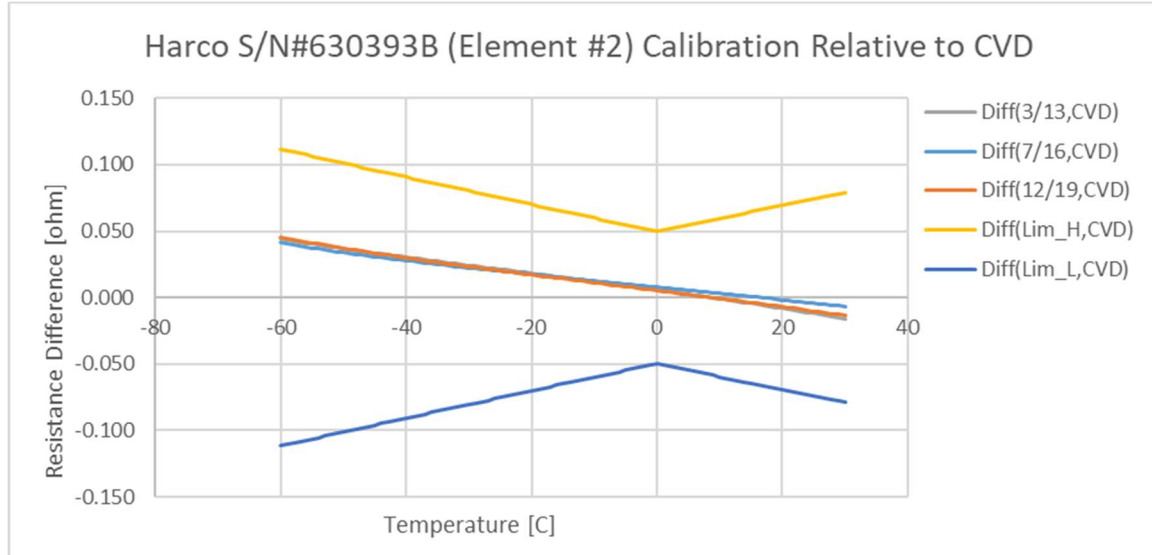


Figure 16 Harco Element #2 calibrations relative to the Ideal CVD curve and including limits per MIL-P-27723E.

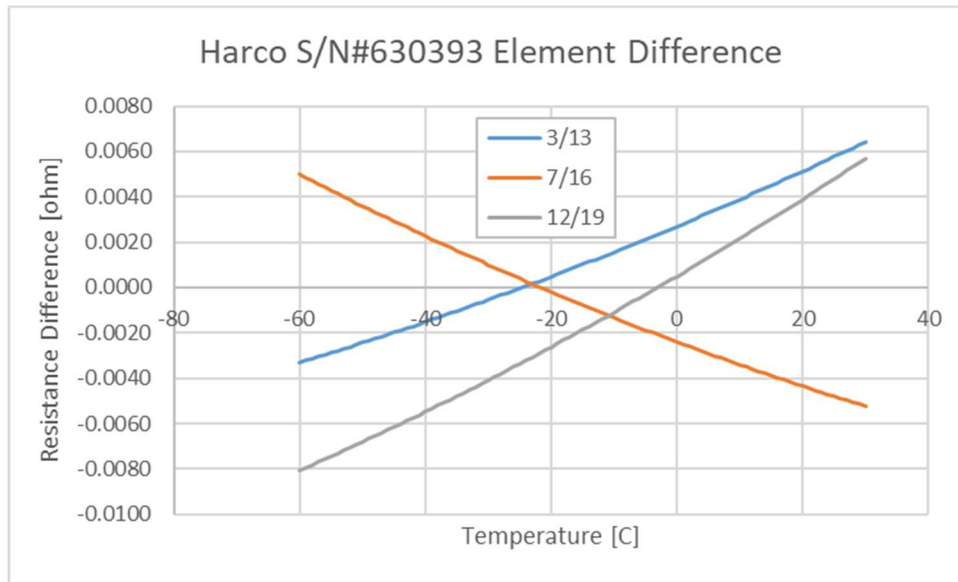


Figure 17 Harco TAT elements #1 and #2 difference measured during calibrations.

Review of the Rosemount 102E2AL non-deiced sensor S/N#3400 bath calibrations is also included here, as it is important for the “Recovery Factor Parameterization Alternate Proposal”. Shown in Figure 18, this unit was calibrated in 2014 and 2016 and showed a near-constant 0.015Ω ($\sim 0.075^\circ\text{C}$) shift between calibrations, significantly more than the Harco sensor calibrations.

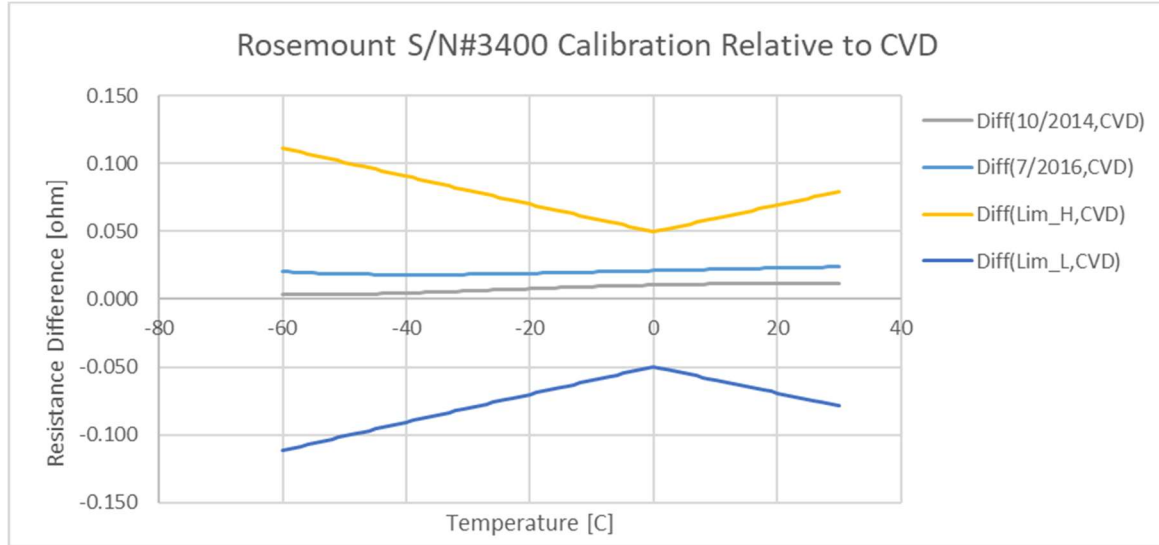


Figure 18 Rosemount 102 non-deiced TAT bath calibration, relative to the ideal CVD curve, and including limits per MIL-P-27723E.

Engineering Calibration

Results from engineering calibrations are included here to justify a change observed after installing the TEMP-DACQ modules. Pre-SPICULE calibrations indicate a $\sim 2^{\circ}\text{C}$ shift in the a0 coefficient for all temperature channels (RTH1, RTH2, RTF1) as shown in Table 4 and Table 5, as they apply to Figure 4. A component used in the original Temperature Amplifiers (LT1010) had a large static offset of $\sim +80\text{mV}$ which resulted in $\sim 2^{\circ}\text{C}$ offset and was compensated by the engineering calibration coefficients. The component was removed from the Modified Temperature Amplifier devices integrated in the TEMP-DACQ Integrated Modules to eliminate this offset, thereby resulting in a $\sim +2^{\circ}\text{C}$ shift to the a0 coefficient.

The RTH1 a0 shift between MethaneAir'21 and ASPIRE'21 of ~ 0.16 is a result of the TEMP-DACQ Module repair explained in the section, “In-Flight Temperature Sensitivity of the Electrical Signal Path”.

Table 4 Engineering calibration coefficients of the Harco S/N#630393 RTH1 and RTH2 channels before and after TEMP-DACQ installation in 2021.

Pre-Campaign Calibration	RTH1			RTH2		
	a0	a1	a2	a0	a1	a2
CSET, 6/2015	-82.2287	22.5752	0.30554	-81.8871	22.5815	0.304795
ORCAS, 11/2015	-82.272	22.604	0.30438	-82.083	22.627	0.30584
SOCRATES, 11/2017	-82.303	22.599	0.3067	-82.118	22.611	0.3097
MethaneAir, 11/2019	-82.3357	22.6539	0.303623	-82.1362	22.6869	0.304457
TEMP-DACQ Install, 1/2021						
SPICULE, 4/2021	-80.6156	22.6495	0.30425	-80.4599	22.6624	0.307519
MethaneAir, 7/2021	-80.6949	22.6521	0.30411	-80.4834	22.6645	0.307055
ASPIRE, 12/2021	-80.5331	22.6494	0.304546	-80.4762	22.6632	0.307074

Table 5 Engineering calibration coefficients of the Rosemount S/N#3400 RTF1 channel.

Pre-Campaign Calibration	RTF1		
	a0	a1	a2
CSET, 6/2015	-82.6043	22.7491	0.307167
ORCAS, 11/2015	-82.457	22.679	0.30876
SOCRATES, 11/2017	-82.491	22.694	0.30952
TEMP-DACQ Install, 1/2021			
SPICULE, 4/2021	-80.3943	22.5055	0.305357

Error (or Change) Analysis Summary

Many contributors of ambient temperature error and compensation have been considered in this signal path analysis, so a summary is provided here for the errors at -30C ambient temperature and Mach 0.8 for the newest signal path to highlight the largest contributors studied in this report in Table 6. A summary of measured TAT sensor discrepancies is given in Table 7. Here, recovery temperature measurement errors are approximated to result in ambient temperature error of same magnitude.

Table 6 Summary of significant errors or recent changes studied in this report

Source of Error (or change)	Raw Error (or change)	Ambient Temperature Error (or change) at -30C, Mach 0.8	Assumptions and source of data
TempAmp Gain temperature dependence error	0.004 °C/°C	0.060°C	15°C TEMP-DACQ box change from calibration condition. See Table 3.
Sensor interconnect cabling temperature dependence error	0.005 °C/°C	0.150°C	30°C Radome air temp change from calibration condition. See Table 3.
Oil Bath Calibration RTH1, RTH2 Historical Changes	+/-0.004 ohms	+/-0.02°C	Figure 17
RTH1 Recovery Factor Change Pre-/Post-2019	0.02	0.04°C	Figure 6 and Figure 8
RTH2 Recovery Factor Change Pre-/Post-2019	0.019	0.5°C	Figure 6 and Figure 8

Table 7 TAT Sensor measurement discrepancies

Measured Discrepancy	Raw Error (or change)	Ambient Temperature Error (or change) at -30C, Mach 0.8	Assumptions and source of data
abs(ATH1 – ATH2)		-0.4 to -0.6 °C/°C	SPICULE data with Post-2019 recovery factor
Measured Electrical Signal Path temperature dependence with Resistor Reference	~0.006 °C/°C	0.15 °C	Figure 14
Difference between measured RTH1, RTH2 recovery factors in the range Mach 0.7 to 0.8	+/- 0.015	+/-0.4 °C	Figure 6 and Figure 8 and Figure 11

The change to the recovery factor models, and the difference between the measured recovery factors estimates stand out to be on the same order as the critical data observations initially noted. The effect of temperature on the interconnect cabling is also notable, whereas the other sources of error have much less significance. Considering the dominant significance of the recovery factor change, and this author's criticism of the underlying analysis that justified the change, a new recovery factor module is proposed.

Recovery Factor Parameterization Alternate Proposal

The analysis of [1] and subsequent changes to the Harco recovery factor parameters introduced a change in the derived ambient temperature that results in optimal matching of the two Harco elements at very cold temperatures (< -50°C) at the cost of worse matching at mid-range temperatures (-40 to 0°C). [1] concludes that the recovery factor of Harco element #1 should be offset from element #2 by ~2% over the entire Mach range. To the contrary, the results from section “Harco Recovery Factor Inter-Comparison” indicate that the elements are not significantly offset in an average sense across the Mach range and that attempts to correct differences between elements do not apply across different sensor heads. This author’s concerns about the Harco recovery factor analysis in [1] include 1) The method of attaining recovery factor from the derivative of recovery temperature was over-simplified²⁵ and the results claim recovery factor greater than 1 for element #1 at high Mach, 2) the analysis results had very large variances due to the large dTr/dX noise, and 3) the method emphasizes conditions of large change rather than steady state conditions.

An alternate proposal given here uses flight data to estimate the recovery factor of the Harco sensor, similar to [1], but uses a different derivation strategy that assumes the Rosemount 102E2AL non-deiced sensor as a truth reference and specifies that both Harco elements must be identically parameterized.

Fundamental Assumptions

- {RTF1} is used as a reference source measurement from which the Harco recovery factors are derived. The Rosemount non-deiced sensor is chosen as truth because its recovery correction is ~3 times smaller than the Harco sensor.
- The {RTF1} recovery factor is assumed equal to the middle value reported in [4] Figure 20 (converted from Recovery Correction) at each Mach value.
- {RTF1} encounters the same mean ambient temperature as {RTH1}, {RTH2} during a 1 second window based on the symmetrical mounting about the GV fuselage.
- The recovery factors of the Harco sensor’s two elements shall be assumed equal, despite the known variation across Mach of S/N#630393. The optimal parameters shall be the average of the two element characterizations.
- The signal paths are well calibrated and the {RTF1}, {RTH1}, and {RTH2} signal paths experience similar error drift across exposure to ambient conditions that largely cancel in the recovery factor estimate.
- The recovery factor model curve is Equation 3, and both C0 and C1 are optimized. C2 and C3 values remain unchanged to maintain a similar curvature to the original Rosemount deiced recovery correction model of Figure 5.²⁶

With these assumptions, Equation 4 leads to Equation 5 where the Harco recovery factor (α_{rH}) is estimated as an adjustment to the Rosemount non-deiced sensor recovery factor (α_{rF}) based on a scaled difference of recovery temperatures. Figure 19 shows that large error in {ATF1} (< 10°C) and {MACHX} (< 0.03) results in insignificant error in the derived recovery factor. Therefore, the derivation accuracy is limited by the assumption of α_{rF} and the recovery temperature measurement accuracies (including calibration and signal path error). A big advantage of this estimation method is that the impact of the error sources is more constrained at higher Mach where the estimation is more important.

$$\alpha_{rH} = \alpha_{rF} - \frac{2c'_v}{R'} \cdot \frac{\{RTF1\} - \{RTHx\}}{(\{ATF1\} + T_0) \cdot \{MACHX\}^2}$$

Equation 5 Derivation of the Harco deiced recovery factor (α_{rH}), using the Rosemount non-deiced sensor as a reference.

²⁵ Equation 4 in [1] does not properly apply the derivative because the recovery factor is not constant. See “Appendix C: Recovery Factor Estimation from Speed Runs”

²⁶ The choice to maintain the C2 and C3 coefficient is somewhat arbitrary because data at Mach < 0.3 is limited and with large variances. The dynamic heating compensation in this regime is also much smaller.

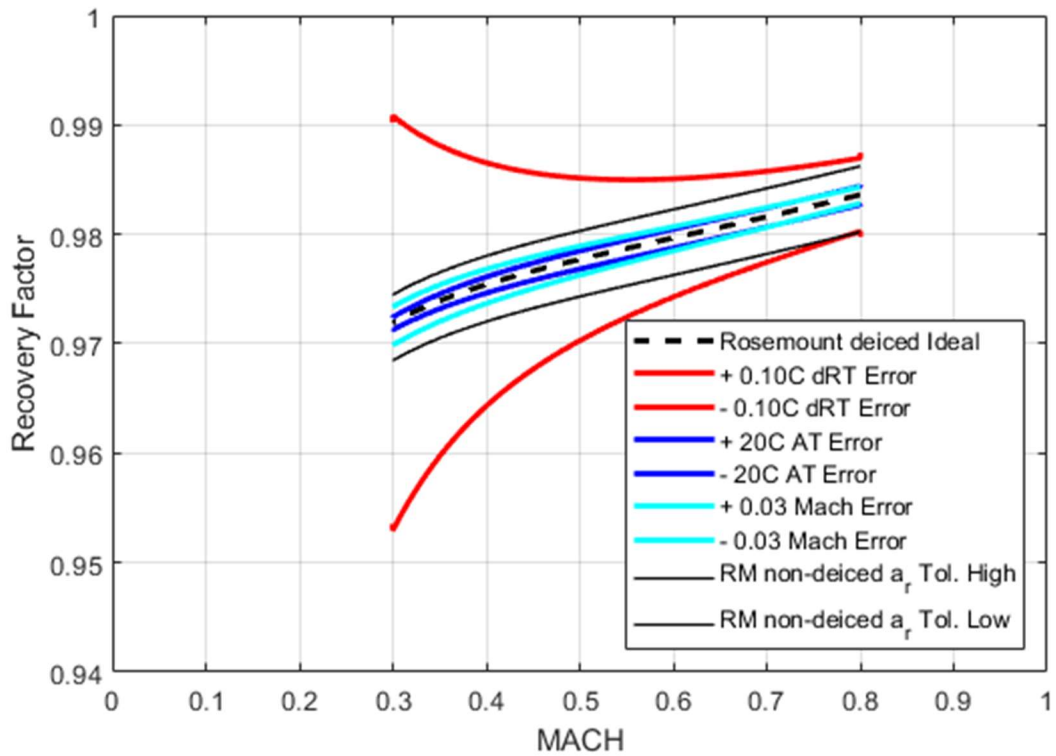


Figure 19 Impact of error sources on recovery factor estimation method, assuming the ideal recovery factor from the Rosemount 102 deiced sensor: +/-0.1C error in the recovery temperature difference, +/-10C error in the ambient temperature, +/-0.03 Mach error, and the error due to Rosemount 102 non-deiced recovery factor tolerance limits [4].

Table 8 Campaign data for recovery factor derivation

Harco S/N#	Rosemount 102E2AL S/N#	Flight Data
630393	3400	CSET (RF02, RF03, RF04, RF05, RF06, RF07, RF09) ORCAS (RF01, RF03, RF04, RF06, RF07, RF08, RF09) SOCRATES (FF02, FF04, FF05, RF03, RF06, RF10, RF11, RF15) SPICULE (RF04, RF05, RF06, RF08)
630393	2932	TI3GER (RF01 – RF06)
708094	2984	DC3 (RF02, RF04, RF07, RF08) TORERO (RF01, RF02, RF03, RF04, RF05)
812452	2984	DEEPWAVE (RF06, RF15, RF17, RF20, RF23)
812452	3109	IDEAS-IV (RF02, RF03, RF09, RF10)

Equation 5 is used to derive the recovery factors for each of the two elements of the Harco sensor based on the following additional processing assumptions:

- Time-domain recovery temperature data are averaged over a 1s window and sub-sampled at 1 Sample-per-second (SPS). This is available as a standard netCDF file from the campaign data repository.
- The {RTHx} data is delayed from {RTF1}, {ATF1} and {MACHX} due to the response time of the Harco sensor. Therefore, the 1Hz {RTF1}, {ATF} and {MACHX} data are filtered by (convolved with) a 1st order low-pass impulse response function with a 2s time constant.²⁷ Filtering the data in this way re-aligns the variables in time and reduces high frequency variation.

²⁷ The 2s time constant specified here is a compromise between the 2.32s re-alignment shift used in [1], and the 1.28s time constant reported in [11], and demonstrates significant reduction in analysis noise.

- The 1SPS recovery temperature data are binned according to {MACHX} values (~ 200 bins), and the data points within each bin are averaged over each flight for each single sensor element. Data for $\{MACHX\} < 0.3$ is ignored. The results are plotted.
- Binned data from all flights and both elements are then averaged together. The model is fit to the averages using a least squares optimization swept across the recovery factor model $\{C_0, C_1\}$ parameter space.
- Data are utilized from the flights in Table 8, chosen for their wide range of flight conditions, to derive the recovery factor and optimize the model across “all flights”. The recovery factor model is also optimized for each separate combination of Harco and respective Rosemount non-deiced sensors.

Generally speaking, using measurements from the fast non-deiced Rosemount to characterize properties of the de-iced Harco sensor inherently links the measurements, sacrificing measurement independence. But, a benefit of this analysis technique is that signal path errors and systematic calibration errors of the two measurements tend to cancel in the numerator due to the similarity of the signal paths, and the equation is very insensitive to the absolute quantities in the denominator. The accuracy of α_{rF} is therefore critical, and as long as the actual fast Rosemount sensor is well represented by the recovery factor characterization tolerance limits in [4], then the α_{rH} estimation is well-constrained, as demonstrated in the simulation results of Figure 19, particularly at Mach > 0.5 .

Flight Data Results

The derived, Mach bin averaged, Harco recovery factor results in Figure 20 have distinct features:

- Element#2 follows the expected curvature better than Element#1 which has large deviations between Mach 0.55 and 0.8. Although not shown here in detail, Mach > 0.75 is very sensitive around 10-12km and is modified by some other unknown dependence, therefore the results here show an average of those states on a per-flight basis. This is also suggested in Figure 11.
- The average recovery factor of both elements is lower than the Rosemount 102E2AL non-deiced sensor for both elements over most of the Mach range.
- Campaign-to-campaign recovery factor variability is approximately ± 0.01 , and campaigns appear offset from one another. Flight-to-flight and bin-to-bin standard deviation is less than ± 0.002 for CSET and SPICULE above Mach 0.5, and approximately ± 0.005 for SOCRATES. SPICULE underestimates the average results, whereas ORCAS overestimates the average and is noisier at high Mach than the other campaigns. CSET and SOCRATES are closer to the average.

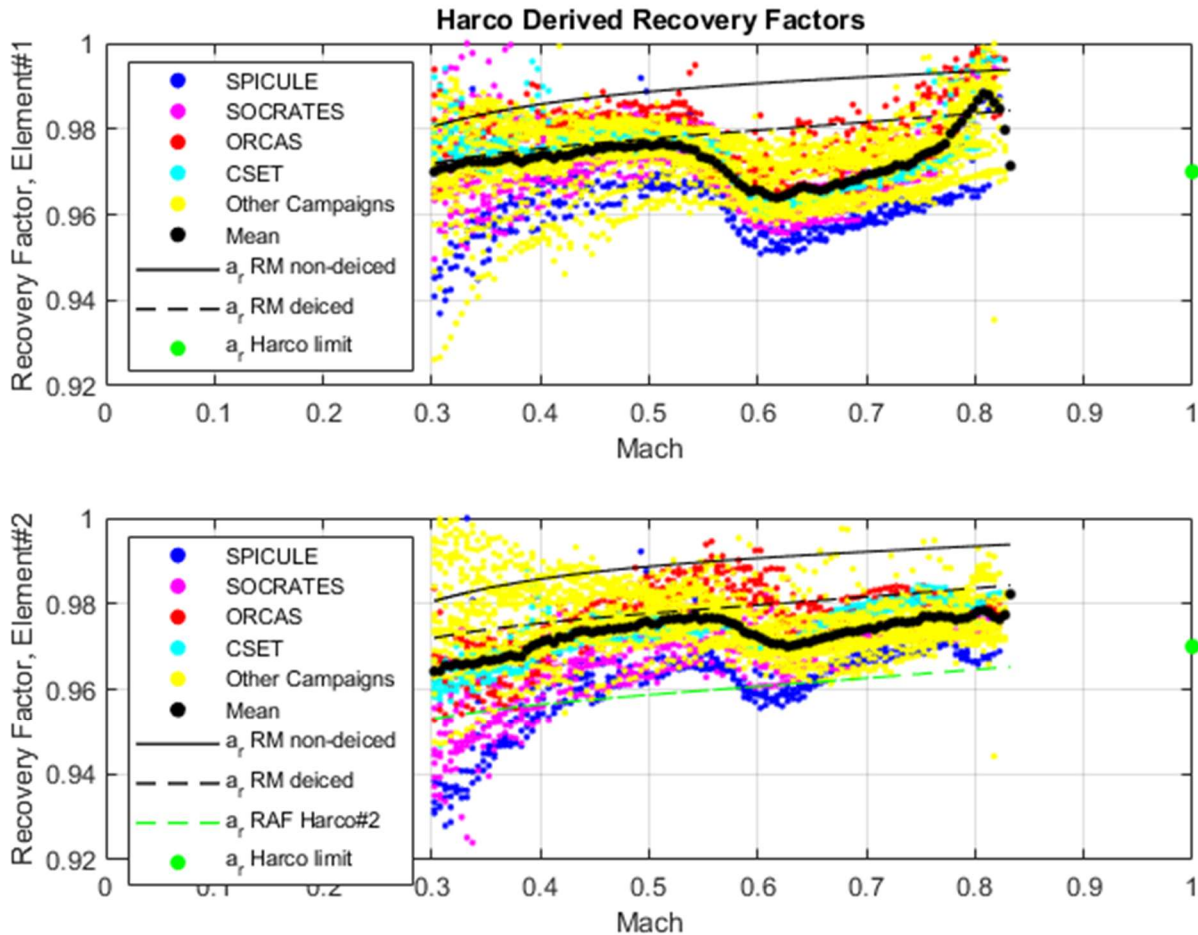


Figure 20 Harco sensor derived recovery factor for elements #1 and #2 across a few sensor units and many campaigns. The ideal recovery factor model of the Rosemount 102 de-iced sensor, Rosemount 102 non-deiced sensor, and the RAF Post-2019 Harco element#2 model are included for reference.

Acknowledging the recent changes to the electrical signal path prior to SPICULE, the ~ 0.01 shift relative to the average in the SPICULE requires justification. Three interesting qualities of the shift are that 1) the shift migrates to lower values from CSET(2015) to SOCRATES(2018) to SPICULE(2021), 2) the shift is large relative to the average offset from α_{rF} , therefore the shift cannot be caused by {MACHX} error, nor {ATF1} error and so must be caused by $\{\text{RTF1}\} - \{\text{RTHx}\}$ or the α_{rF} assumption, and 3) the shift appears almost constant across Mach and similar for both elements.

A constant shift and the $1/\{\text{ATF1}\}/\{\text{MACHX}\}^2$ relationship of Equation 4 requires that the recovery temperature difference error is smaller at low flight speeds (typically high ambient temperature) and grows at higher speeds (typically low ambient temperature). The shift approximately corresponds to $\sim 0.13^\circ\text{C}$ error at Mach 0.4 and $\sim 0.4^\circ\text{C}$ at Mach 0.8. These qualities are potentially explained by static gain errors or temperature dependent signal path errors, although temperature dependent signal path errors are less likely because they usually have a very long lag time (10's of minutes) relative to the ambient temperature.

A more compelling explanation is that the Rosemount reference sensor changed over time. Repeating the analysis with the “avionics” temperature $\{\text{RT_A}\}$ substituted in place of $\{\text{RTHx}\}$ in Equation 5 also shows a ~ 0.01 offset in the derived recovery factor for SPICULE. If the Harco recovery factor is derived with $\{\text{RT_A}\}$ as the reference source, the derived values align more closely for CSET, SOCRATES, and SPICULE from 0.5 to 0.8 Mach, and for both elements. By removing the Rosemount non-deiced sensor from the analysis, the SPICULE offset disappeared. Although the avionics temperature sensor recovery factor and measurement accuracies may have significant errors or unknowns, its permanent installation and untouched data processing likely have good consistency over time. The fragility of the Rosemount 102 non-deiced

element may lead to poor consistency over time, which is supported by the bath calibration results of Figure 18. Therefore, the SPICULE shift of Figure 20 may be due to changes to α_{RF} , the {RTF1} measurement, or the element's resistance vs. temperature characteristic since it was last calibrated in 2016.²⁸ This observation challenges the initial assumption of using {RTF1} as a truth reference, but the recovery factor error caused by the SPICULE shift would be < 0.002 due to averaging over many campaigns, which should be acceptable.

The explanation for the shift during SPICULE may remain unknown. Future campaigns may confirm the shift to be permanent and true, or it may be in error due to the reference measurement. In fact, data from the TI3GER'2022 campaign more closely resembled the data from CSET. Weighting the recovery factor optimization to favor (or disfavor) the SPICULE data cannot be justified at this time.

The noisiness of the ORCAS data might be explained by its wide-ranging flight profiles, frequently descending low and then ascending back to very high altitudes, which is very susceptible to signal path error temperature dependence. No attempt is made here to investigate offset.

Parameter Optimization

Averaging together the data from all flights and both elements and fitting the model to the data results in Figure 21 with the recovery factors of the Rosemount 102 deiced and non-deiced sensors [4] included for comparison. 2-sigma Confidence Intervals are within +/-0.01 of the mean and +/-0.17 from the model curve fit above 0.5 Mach. Element#1 has more variation than element #2. Figure 21 also shows how RAF's Post-2019 model for Harco Element#2 (labeled as 'ar RAF Harco#2' in the figure) lies at the edge or outside of the data confidence interval.

The optimization was also repeated individually for the different combinations of Harco and Rosemount non-deiced combinations (albeit with the smaller data sets of Table 8), and the model curve fit coefficients from all cases are given in Table 9.

After re-deriving the ambient temperature data for all flights using the optimal recovery factor coefficients for Harco S/N#630393, {ATH1} and {ATH2} are subtracted from {ATF1} in the following table of figures for a variety of flights. The figures show a comparison between derived measurements for the pre-2019, post-2019, and proposed parameters. The proposed parameters reduce the difference to below 0.5°C across all results, with significant improvement in the -40 to +30°C range.

²⁸ The {RTF1} consistency argument warrants investigation of the S/N#3400 sensor, although an icing incident in the final SPICULE flight likely damaged the element and changed its characteristics.

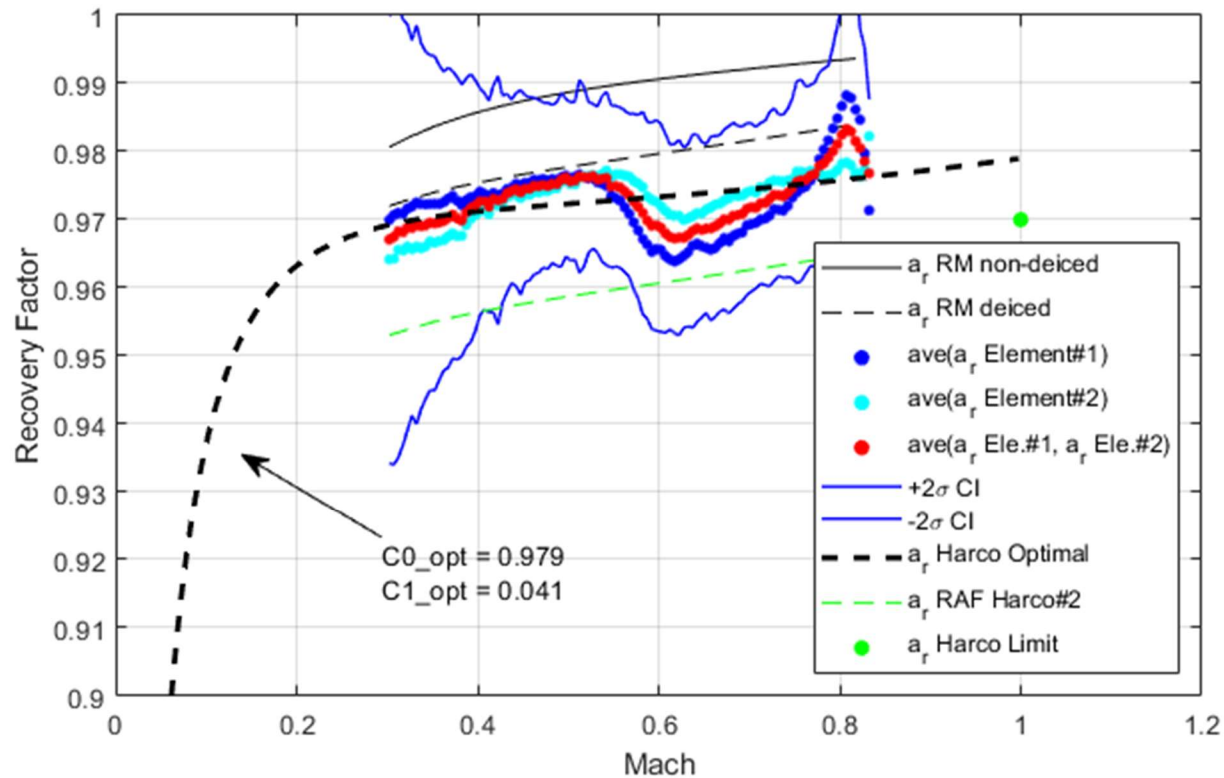
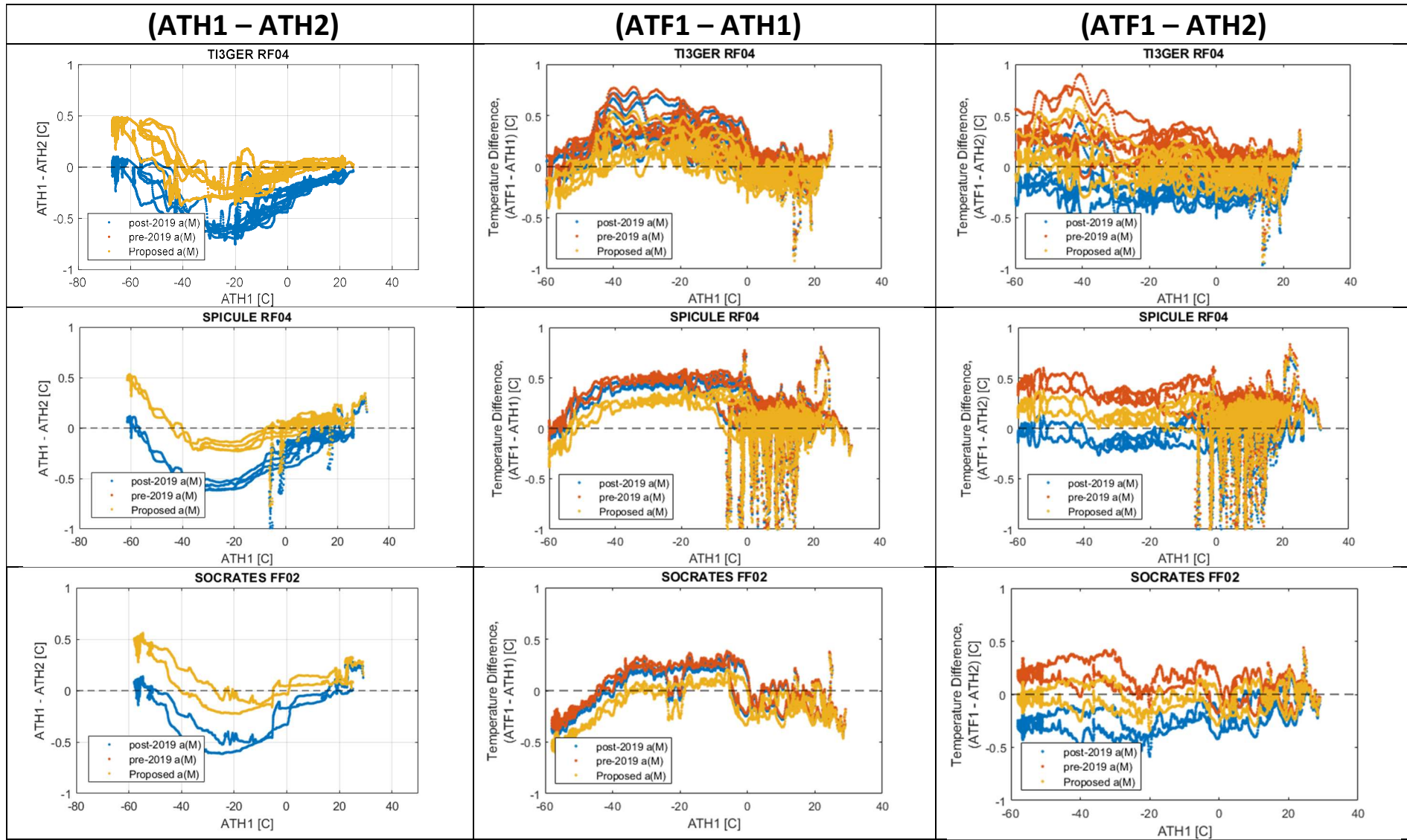


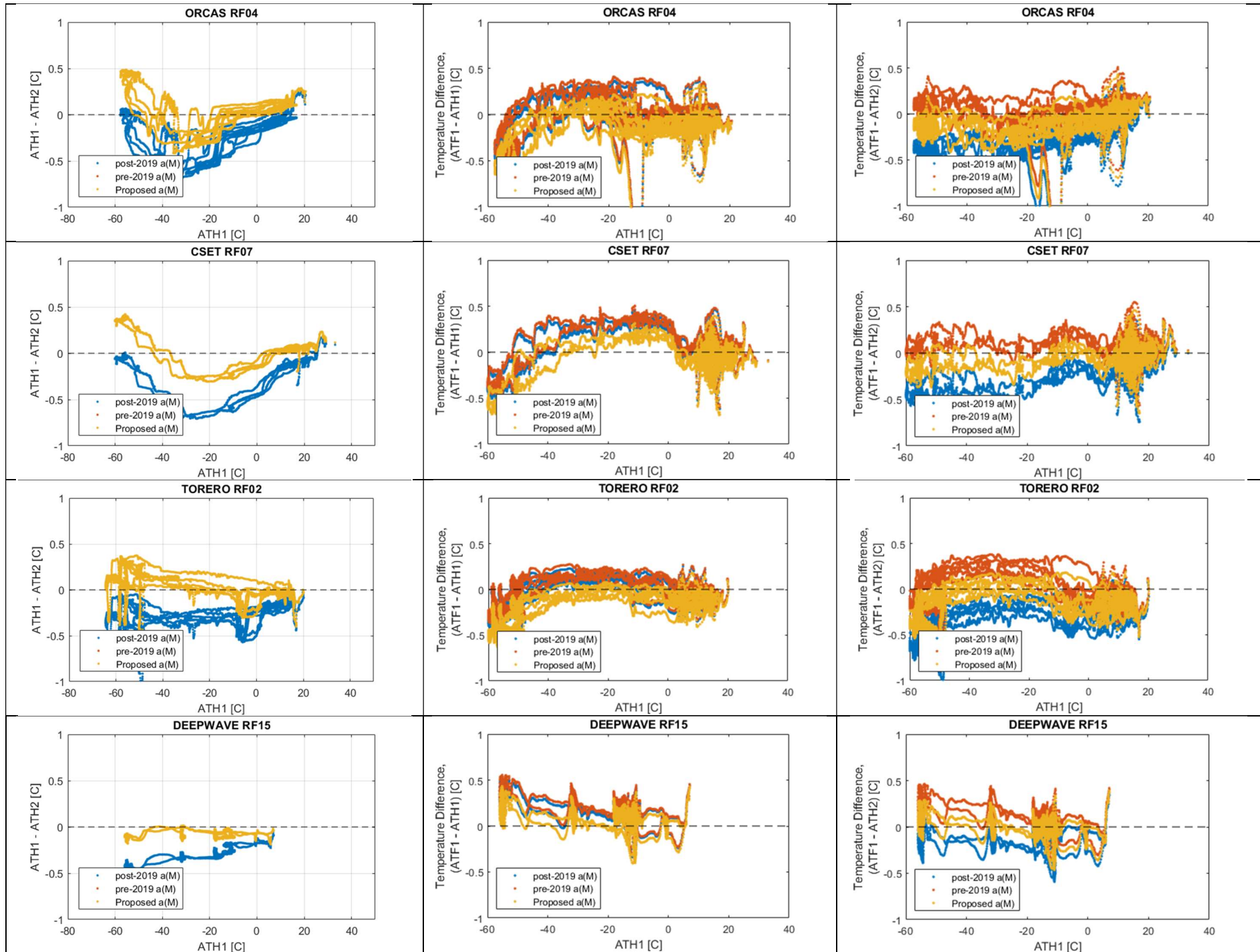
Figure 21 Optimized Harco recovery factor model based on average of all flights. 2-sigma confidence intervals shown indicating the data variation.

Table 9 Recovery factor model {C0, C1} parameters derived for a few Harco sensors.

Campaigns	Harco de-iced S/N#	Rosemount non-deiced S/N#	C0	C1
SPICULE, SOCRATES ORCAS, CSET	630393	3400	0.981	0.052
TI3GER	630393	2932	0.978	0.04
DC3, TORERO	708094	2984	0.983	0.04
DEEPWAVE	812452	2984	0.977	0.041
IDEAS-IV	812452	3109	Large data errors ²⁹	
ALL FLIGHTS	-	-	0.979	0.041

²⁹ Data from IDEAS-IV appears reasonable in the time domain but has wildly varying derived recovery factor variation.





Other Potential Areas of Concern

3-Wire Detection Circuit

The electrical signal path utilizes a 3-wire resistance sensing method that contributes error due to voltage drop across the temperature dependent cable resistance ($\sim 250 \text{ m}\Omega + 1 \text{ m}\Omega/\text{ }^\circ\text{C}$) of the return current path that can lead to a $0.3\text{ }^\circ\text{C}$ shift over a $60\text{ }^\circ\text{C}$ radome ambient temperature range. Strategies exist to characterize 3-wire circuit resistance during calibration and eliminate the error from measurements, but these are not implemented, nor has a strategy been identified that is feasible for the existing hardware setup. A 4-wire circuit (2 current wires and 2 sense wires) solves the problem by preventing current flow in the sensing wires. A 4-wire circuit may be possible in the GV but would require the following substantial hardware changes.

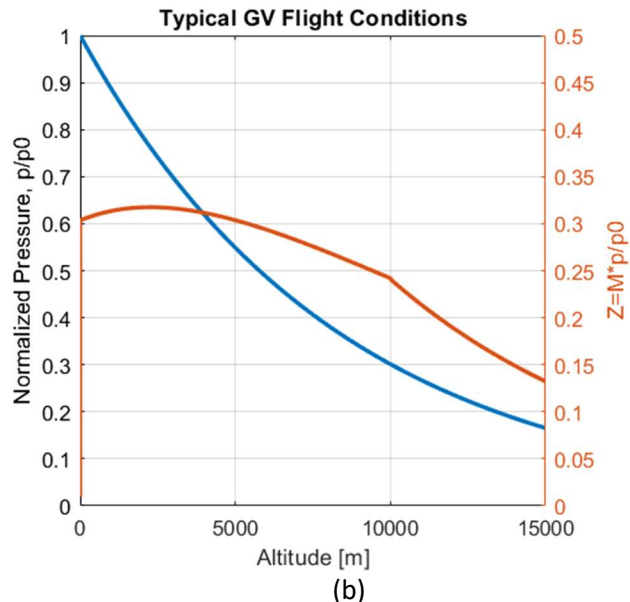
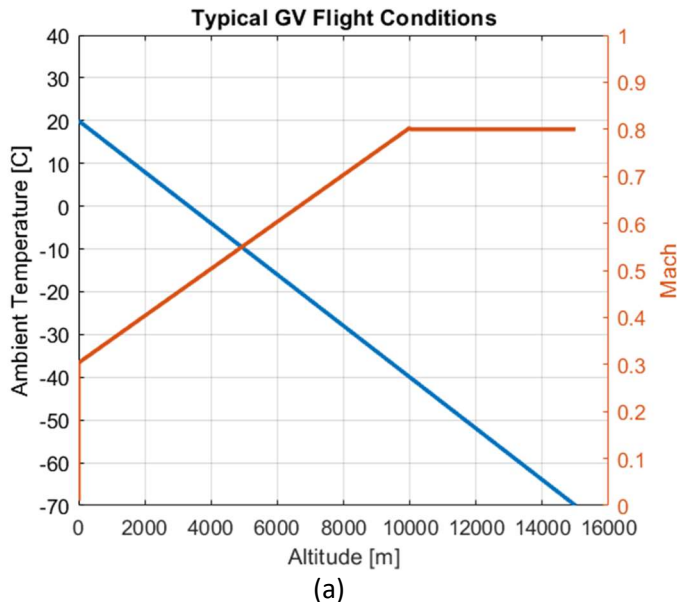
- Redesign the TEMP-DACQ Integrated Module to implement a 4-wire design. Requires changes to the Temperature Amplifier PCB, TEMP-DACQ PCB, and module connectors.
- Modify the connectors on the GV Radome Environmental box to accommodate the added signals.
- Replace all analog temperature channel interconnect cabling in the radome, including expanding to larger connectors at the environmental box interface.

Deicing Heat Error

The difference between the elements of the Harco S/N#630393 sensor and the derived recovery factor curves both show strong divergences above 10km where $\text{Mach} > 0.75$, for example, in Figure 22 (d). Most of the divergence occurs for element#1. A possible explanation for these discrepancies is deicing heat error. At high altitudes, the air mass flow is reduced so the deicing heat error is larger, as indicated in Figure 22 (c) from [4]. Assuming typical GV flight conditions of Figure 22 (a), Figure 22 (b) shows that typical flight conditions occur around the “knee” of the deicing heat error curve, with large changes at altitudes above $\sim 9\text{ km}$. At 13.6km the de-icing error can be between 0.2 to 1.0C with a typical 0.6C value. [4] recommends turning off deicing heat above $\sim 9\text{ km}$.

This explanation is supported by the observation that $\text{abs}(\{\text{ATF1}\}-\{\text{ATH1}\})$ often decreases at higher altitudes for Harco S/N#630393 element#1. Other units have a similar trend, but not necessarily starting in the same conditions. A challenge to this explanation is the idea that both elements should be affected by the deicing heat error similarly, and the data does not show similar trends in all cases. Element#2 of S/N#630393 does not show the trend. Both elements of S/N#708094 do show the trend. S/N#812452 does not significantly show the trend in the available data.

Deicing heat error may explain the accuracy deviations to hotter temperatures at high altitude of the Avionics Rosemount sensor data, and the Rosemount deiced sensor flown during CONTRAST [9].



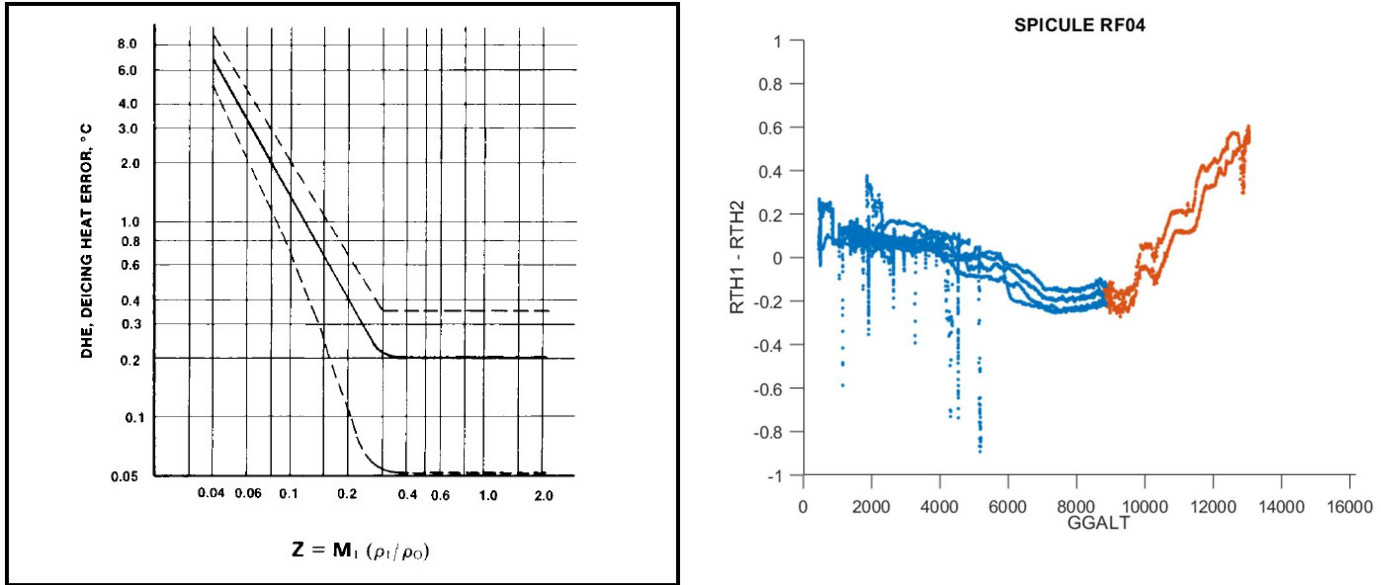


Figure 22 Effects of De-icing heat on Rosemount 102 deiced sensor accuracy. (a) Typical GV flight conditions, (b) Z-parameter during typical flight conditions, (c) Deicing heat error vs. Z-parameter from wind tunnel data for Rosemount Model 102 sensors [4] indicating heating error becoming significant at $\sim 10\text{kft}$, (d) Harco element-to-element error vs. altitude during SPICULE RF04 showing divergence above 10kft (where orange indicates $\text{Mach} > 0.75$)

Conclusions

- Bath calibrations of the Harco S/N#630393 sensor have been very stable since 2013. Bath calibrations of the Rosemount S/N#3400 sensor are not as stable, showing a $15\text{m}\Omega$ (0.075°C) shift between 2014 and 2016.
- Replacement of the electrical signal conditioning and data acquisition subsystems with the TEMP-DACQ Integrated Module significantly improved the uncalibrated accuracy and reduced the temperature dependence of the signal path. An issue related to an instance of a bad connector was resolved with a modification to the module, and the change is recommended for all other TEMP-DACQ units.
- Experimental measurements were performed to determine the signal path dependence on temperature using fixed high accuracy resistive terminations in place of the TAT sensors. Results showed high correlation of recovery temperature error with radome temperature ($0.0065^\circ\text{C}/^\circ\text{C}$) which is dominated by the copper resistance temperature dependence of the radome interconnect cabling. Total error during the experiments remained $< 0.21^\circ\text{C}$ across all flight data during ASPIRE'21.
- The new analysis and optimization of the Harco recovery factor concludes the following:
 - The improvements of Harco element data matching at temperatures $< -55^\circ\text{C}$ occurred as a result of the 2019 recovery factor parameter changes and resulted in more error between 0 and -40°C .
 - The maximum recovery factor error caused by poor modeling is approximately 3% at Mach 1.0, as specified by the vendor.
 - Data from different Harco sensors shows sensor-to-sensor recovery variability error $< +/-1.5\%$ over the Mach range that is not consistent from sensor to sensor. This data does not indicate an element-to-element recovery factor offset.
 - Deriving the recovery factor for one sensor unit via Equation 5 and fitting to the model of Equation 3 shows campaign-to-campaign variability of $+/-1.0\%$ (using the same sensor) from the mean, flight-to-flight variability of $< +/-0.5\%$ (in the same campaign), and Mach bin-to-bin variability of $+/-1\%$ after optimal fitting. The total variability is approximately $+/-2.0\%$. This total variability is approximately equal to $+/-0.55^\circ\text{C}$ at Mach 0.8 (-60°C) and $+/-0.27$ at Mach 0.5 (-20°C) and likely includes contributions from other error sources.
 - The amount of variability after optimization, relative to the maximum recovery factor error specified by the vendor (3% at Mach 1.0), suggests that the accuracy improvement is only marginal compared to a

- rough estimate of the model assuming half the maximum error. In fact, the optimization method presented here settled on a solution equivalent to approximately 2/3 of the maximum error.
- Analyzing the recovery factor derivation of Equation 5 using different temperature channels as references suggests that the Rosemount S/N#3400 characteristics may have shifted since the previous bath calibration in 2016.
 - The good matching of {ATH2} to {ATF1} during SPICULE is NOT justification to prefer {ATH2} over {ATH1} for the {ATX} variable, and is not supported by previous campaign data. A shift in the Rosemount non-deiced sensor S/N#3400 is suspected, and updating the Harco model parameters to reflect the new optimization will change the matching observation.
 - The new Harco proposed recovery factor model is recommended for campaigns going forward. Applying the optimization to past campaigns requires more input from the RAF science team.
- Harco sensors show strong divergence for some elements above ~10km, in the regime where deicing heat error can become large (approx. 0.2 – 1.0°C) for Rosemount Model 102 sensors. Deicing heat error is not currently compensated, and characterization data of the Harco probe is not available. The error may be mitigated by disabling deicing heat above 9km.

Recommendations 9/2021

- Change the Harco recovery factor model {C0, C1, C2, C3} parameter values to {0.979, 0.041, 0.090, 0.091}
- Return the Rosemount deiced {C0, C1, C2, C3} parameter values to {0.988, 0.053, 0.090, 0.091}
- The author does not recommend individually parameterizing the recovery factor for each sensor unit (of the same model) individually due to the susceptibility of the characterization to other sources of error.
- Perform Rosemount S/N#3400 Bath calibration. Also perform a bath calibration of the back-up unit if #3400 is irreparably damaged.
- Investigate methods for, and effectiveness of, disabling Harco deicing heat above 9km.
- Acknowledge that the ambient temperature difference error is larger at higher Mach, with possible error of +/- 0.5°C at Mach 0.8 for the Harco sensors, even after recovery factor optimization.
- Change the primary (right-side) Harco sensor to S/N#708094 or S/N#812452 to eliminate the difference pulses and reduce the sharp variances in the recovery factor response from the expected curve.

Appendix A: RTH1-RTH2 Pulses

Harco sensor data occasionally contains ($\{RTH1\} - \{RTH2\}$) “difference pulses” with a step change of 0.1 to 1.3C (that may or may not completely settle) followed by relaxation to the original value. One unique ~25s long example was observed during MethaneAir’2021 RF06 (shown in Figure 23 (a)&(b)), and a more common ~7s example was observed during OTREC’2018 RF08 (shown in (c)&(d)). Instances can also be observed in campaigns long passed including ICEBRIDGE and NOREASTER. The instances have many common properties:

- The step and relaxation response rate is similar to the known time response of the Harco sensor (~1-2s).³⁰
- Single isolated pulses occur exclusively at very high altitude (>11km) and low temperature (<-55C). Single pulses sometimes occur in ascent/descent pairs with one at the beginning and end of a high altitude flight leg (MethaneAir’21 RF08, SPICULE RF04, ORCAS FF01, NOREASTER FF01).
- Sustained bunches of pulses may occur during flight legs at a high altitude (MethaneAir’21 RF06, ORCAS RF07, CSET RF01) as shown in Figure 23 (e)(f)(g)(h), sometimes in the presence of semi-coincident water content (OTREC FF02, DC3 RF02).
- $\{RTH1\}$ typically decreases in values, while $\{RTH2\}$ increases in value.³¹
- All reviewed data indicates the pulses are specific to Harco S/N#630393. Simultaneous measurements did not show pulses for Rosemount deiced S/N#A50738 (ICEBRIDGE FF04/RF02, NOREASTER FF01), nor a separate Harco S/N#812452 (ACCLIP-TEST TF03), nor Rosemount non-deiced S/N#3245 (PACDEX RF02). No similar pulse phenomena were observed during CONTRAST during which a Harco S/N#812452 and Rosemount deiced S/N#A50738 were flown with ample time at high altitudes.

Some of the sustained bunches add a very large amount of noise to the measurement, and the phenomenon appears to be unique to S/N#630393 but not related to the right-side position signal path that it is always installed in. Changing the primary sensor to S/N#708094 or S/N#812452 may be a reasonable solution, both in terms of eliminating the occurrence of pulses and benefitting from a flatter derived recovery factor.

Potential theories include cable or contact resistance fluctuation at cold temperature, sensor mechanical stress that impacts resistance at cold temperature, instances of acoustic resonance or unique turbulence within the cavity, or ice water content melting on the elements.

³⁰ A separate type of error pulse has been observed from S/N#630393 with instantaneous response and dominated by $\{RTH2\}$. Examples include MethaneAir’2019, SOCRATES, and ORCAS FF03. These appear to be due to a signal path continuity problem, and have not been observed after the TEMP-DACQ installation.

³¹ One interesting example of the reverse case occurred during ORCAS RF07 at 17:05 and ~7.3km near a discontinuity in the ($\{RTH1\} - \{RTH2\}$) vs. GGALT curve.

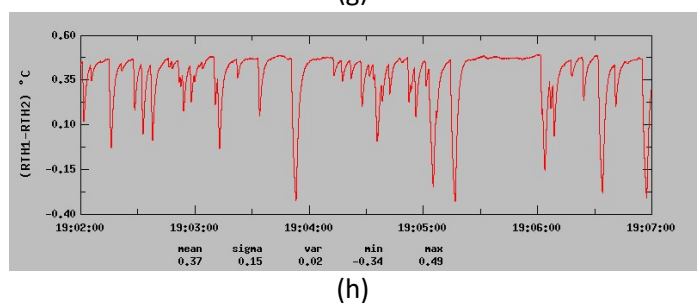
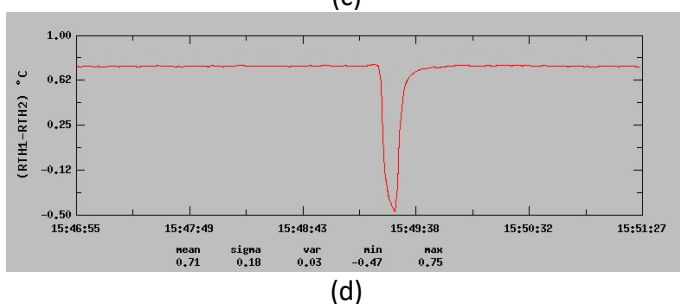
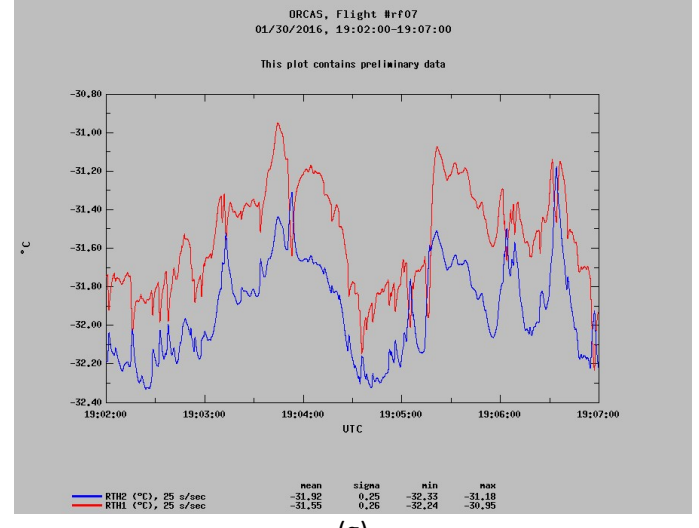
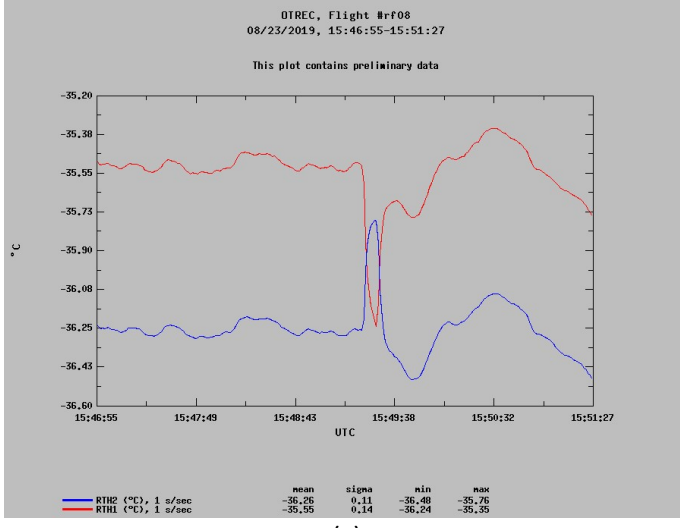
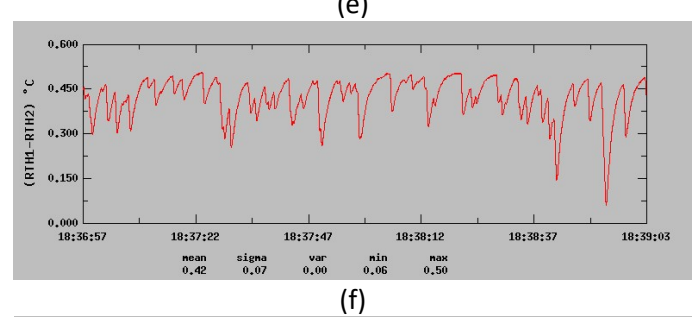
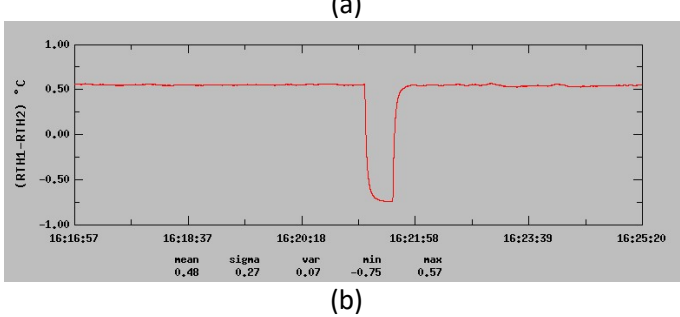
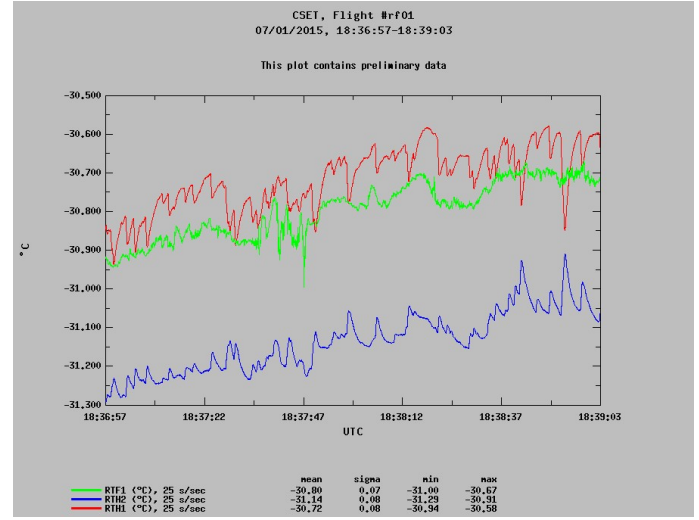
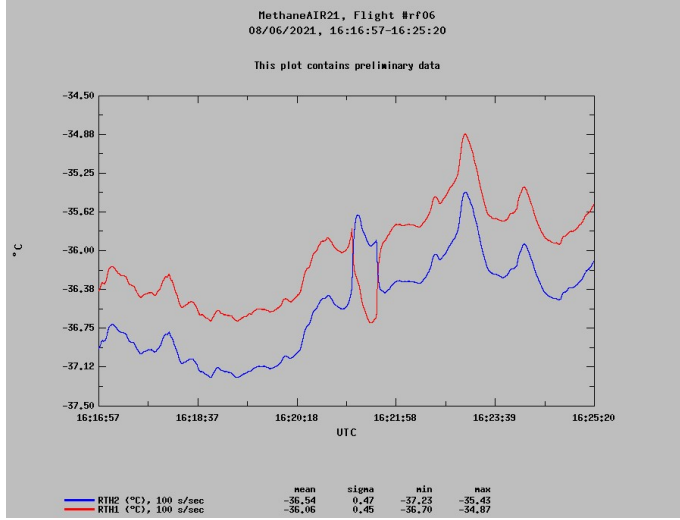


Figure 23 Instances of $(RTH1 - RTH2)$ pulses, with plots of raw data and difference data. (a)(b) 25s long pulse during MethaneAIR RF06, (c)(d) 7s long pulse during OTREC RF08, (e)(f) series of pulses during CSET RF01, and (g)(h) series of pulses during ORCAS RF07. All data corresponds to Harco sensor S/N#630393.

Appendix B: Rosemount 102 Deiced Sensor Performance

The performance of the Rosemount 102CA2W dual-element deiced sensor S/N#A50738 was deemed less accurate in 2014 due to data collected that year during CONTRAST relative to measurements from the simultaneous Harco and avionics sensors [9]. Current records tag the sensor as “Bad after CONTRAST; don’t use.” Despite the large (\sim 1-4°C) offsets from the other measurements, S/N#A50738 has remarkably good in-flight element-to-element measurement matching across the full ambient temperature range, as evident in Figure 24. The sensor unit also demonstrated very consistent bath calibration from 2/2013 (pre-CONTRAST) to 3/2014 (post-CONTRAST). Although the element-to-element difference was \sim 18m Ω , the resistance was within limits and the measurement was repeatable (Figure 25 and Figure 26). This unit is the only Rosemount dual deiced sensor unit that has flown as a research installation on the GV or C130 over the last 12 years or more.

Measurements during CONTRAST were affected by a signal path offset drift that was attributed to the ADC, occurring for both research sensor heads when compared to the avionics sensor [9]. Diagnostic calibrations during the project confirmed a shift in some ADC channels. The ADC card used during CONTRAST (S/N#1704) has only been calibrated in 2011 according to the RAF calibration database. The correction coefficients derived from ADC calibration typically corrected for 100-300mV of offset error and 5-10% gain error. Eight adjustments were made to the Engineering Calibration coefficients during CONTRAST in an attempt to compensate for the drift, and the ADC card was changed to S/N#1710 for the subsequent campaign, DEEPWAVE. Around this time, a design flaw was identified in the ADC design; a potentiometer that trimmed a critical voltage offset was found to shift over time that would cause a global shift of all channels, therefore many cards were modified to eliminate the potentiometer and were recalibrated in 4/2014 (post-CONTRAST), including S/N#1710. Many independent diagnostic voltage references were available on the ADC cards to identify calibration problems, but shifts in these cards are not escalated by technician staff as an issue unless the error approximately exceeds 10mV (corresponding to 0.25°C)³².

The post-CONTRAST data analysis of [9] sought to correct two sources of error simultaneously: 1) signal path offset drift, and 2) resolve the discrepancy between the Harco and Rosemount sensors by determining which was more accurate. #1 applied a per-flight offset correction based on the shift relative to the avionics measurement {AT_A} between RF06 and RF13. #2 assumed a hydrostatic equation-based temperature model as a truth reference and optimized new Engineering calibration coefficients that would fit the data to the hydrostatic temperature model. The analysis concluded that the Harco sensor data required less adjustment to optimally match to the model, therefore the Harco measurement was deemed more accurate than the Rosemount sensor. The Rosemount sensor flew again during NOREASTER’2015 with similar results, and for the last time. No further analysis was attempted to explain the discrepancy of the Rosemount sensor during these campaigns.

Use of the hydrostatic equation temperature model as truth in [9] included many dependent variables (static pressure, vertical velocity, gravity) with many compensations (gravity compensation, pressure compensation based on results from LAMS, gas constant moisture compensation, baroclinic atmosphere compensation), and leaned very heavily on averaging and regression techniques to reduce static pressure precision error. The conclusion also relied on the recovery model of the probes, which would later be adjusted in the 2015 analysis [1].

Following [9], analysis of the Rosemount deiced sensor in [1] concluded a need to adjust the recovery factor by 3% despite that adjustment placing the recovery correction curve outside of the limits specified by the vendor [4]. This adjustment reduced the discrepancy observed in CONTRAST by presuming the recovery factor was in error.

Analysis by this author attempted to reproduce the conclusions of the Harco vs. Rosemount analysis using the hydrostatic equation (albeit by a different method) and confirmed the results of [1]: that the Harco probe is better matched to the hydrostatic equation as truth during the CONTRACT campaign.

Deicing heat error is one likely explanation for the deviation in Rosemount deiced sensor accuracy, which is clearly documented in [4] and yet is neither compensated, nor acknowledged at RAF in recent analyses. One theory is that the

³² Per a conversation with a lead RAF technician, ~2017.

Harco probe is affected by deicing heat error less than the Rosemount, and that some amount of deviation observed in CONTRAST [9] is deicing heat error. From this author's observations, the Rosemount deiced sensor has many qualities superior to the Harco probe that justify attempting to characterize and understand the Rosemount sensor more accurately.

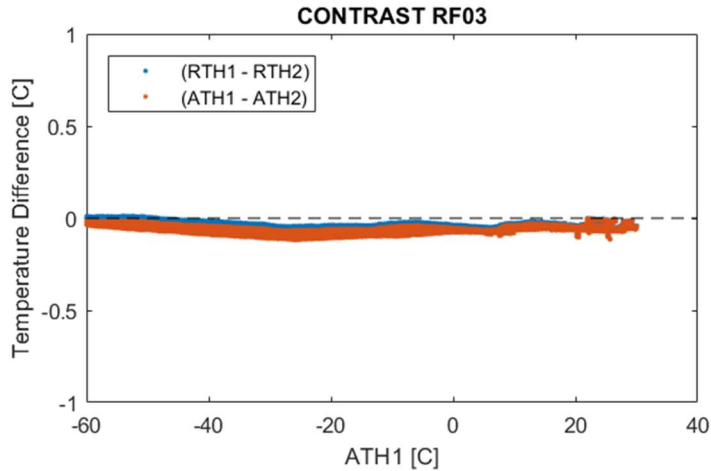


Figure 24 Rosemount 102 deiced S/N#A50738 in-flight element-to-element measurement matching.

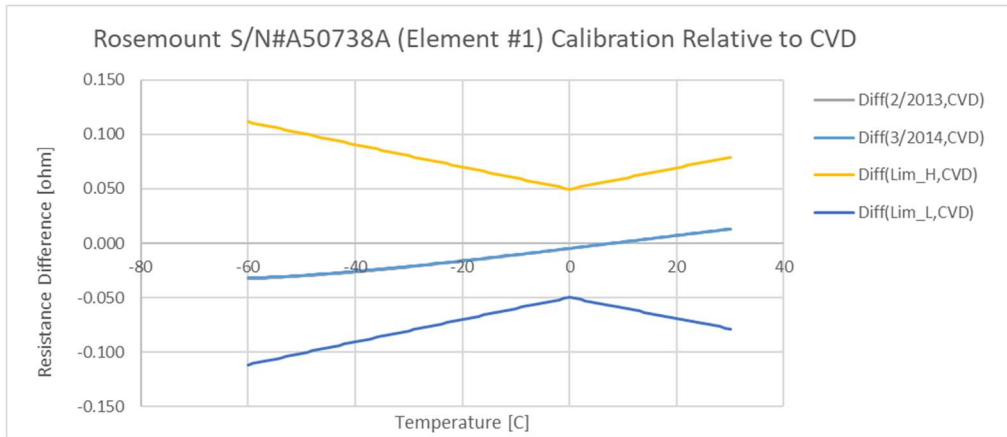


Figure 25 Rosemount 102 deiced S/N#A50738 element#1 oil bath calibrations.

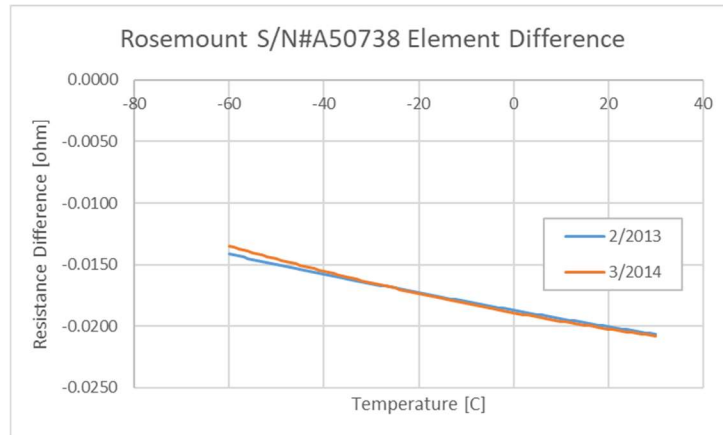


Figure 26 Rosemount 102 deiced S/N#A50738 bath calibration element-to-element difference

Appendix C: Recovery Factor Estimation from Speed Runs, Derivation

Assuming a technique similar to [1], where the recovery factor is derived from the derivative of recovery temperature with respect to Mach, a more rigorous derivation of the recovery factor estimate is as follows without a change of variables. Some of the terms are assumed to be zero during speed runs, and thus eliminated.

$$\begin{aligned}\frac{dT_r}{dM} &= \frac{d}{dM}(T_a + a_r M^2 T_a K), \quad K = \frac{R'_d}{2c_v} \\ \frac{dT_r}{dM} &= \underbrace{\frac{dT_a}{dM}}_0 + a_r 2MT_a K + \frac{da_r}{dM} M^2 T_a K + \underbrace{a_r M^2 K \frac{dT_a}{dM}}_0 \\ a_r &= \frac{1}{2MT_a K} \cdot \frac{dT_r}{dM} - \frac{M}{2} \cdot \frac{da_r}{dM} = \frac{1 + a_r M^2 K}{2MT_r K} \cdot \frac{dT_r}{dM} - \frac{M}{2} \cdot \frac{da_r}{dM} \\ \rightarrow a_r \cdot \left(1 - \frac{M}{2T_r} \cdot \frac{dT_r}{dM}\right) &= \frac{1}{2MT_r K} \cdot \frac{dT_r}{dM} - \frac{M}{2} \cdot \frac{da_r}{dM}\end{aligned}$$

For the $\frac{dT_a}{dM} \sim 0$ assumption to be valid during a speed run and achieve recovery factor error $< 0.5\%$, then $\left|\frac{dT_a}{dM}\right| < 0.005 \left|\frac{dT_r}{dM}\right| \rightarrow \left|\frac{dT_r}{dM}\right| > 200$ must be true but is not always satisfied during a single speed run due to atmosphere variation. Averaging can reduce this requirement, but regardless, this assumption results in large variance.

An approximation may be made if the recovery factor is near constant, which seems intuitive for Mach 0.3 to 1.0. Equation 4 [1] appears to be equivalent to this approximation after resolving the change of variables.

$$\begin{aligned}\frac{dT_r}{dM} &= \underbrace{\frac{dT_a}{dM}}_0 + \underbrace{a_r 2MKT_a}_{large} + \underbrace{\frac{da_r}{dM} M^2 KT_a}_{small} + \underbrace{a_r M^2 K \frac{dT_a}{dM}}_0 \\ a_r &\sim \frac{1}{2MT_a K} \cdot \frac{dT_r}{dM} \\ \rightarrow a_r \cdot \left(1 - \frac{M}{2T_r} \cdot \frac{dT_r}{dM}\right) &\sim \frac{1}{2MT_r K} \cdot \frac{dT_r}{dM}\end{aligned}$$

With this approximation, by comparing the eliminated small term relative to the large term, the recovery factor can be shown to be overestimated by 4-7% over typical values (assuming da_r/dM similar to the Rosemount recovery factor model in [4]) which is too large for this analysis. A potentially more accurate approach would be to use the full recovery factor derivation and approximate $\frac{da_r}{dM} \sim 0.016$ per the Rosemount recovery factor model from Mach 0.4 to 0.8, although the approximation is likely invalid below Mach 0.4 due to high uncertainty of the model at these values.

In general, the analysis is susceptible to very large dT_r/dM noise because Mach does not change rapidly relative to its noise between time points, therefore the denominator can be very close to 0. Fitting Tr vs. M to a polynomial during the speed run (similar to what was done in [1]) works around that problem, but the number of points (<100 for some speed run instances) may not suppress the noise sufficiently. [1] asserted that many speed runs were necessary to get a good mean estimate of the recovery factor in all Mach bins.

References

- [1] A. Cooper, "Study of the Recovery Factor," NCAR RAF, Boulder, CO, 2015.
- [2] A. Cooper and D. Friesen, "Temperature Reprocessing," NCAR RAF, Boulder, CO, 2014.
- [3] "MIL-P-27723E, Section 3.4.2," [Online]. Available: <http://mil-spec.tpub.com/MIL-P/MIL-P-27723E/MIL-P-27723E00006.htm>. [Accessed 7 September 2021].
- [4] "Total Temperature Sensors, Technical Report 5755," Goodrich, 1994.
- [5] "TAT Sensor, Drawing 100989, Rev.D," Harco Laboratories, Inc., 2/24/2005.
- [6] J. Carnes, "Temp Amp Dacq Design Review.pptx," NCAR RAF, 12/2018.
- [7] J. Carnes, "xDACQ Users Guide," NCAR RAF, Boulder, CO, 2021.
- [8] A. Cooper, "A/D Calibration," NCAR RAF, 5/2009.
- [9] A. Cooper, "Temperature Measurements in CONTRAST," NCAR RAF, Boulder, CO, 3/2014.
- [10] RAF, "RAF Technical Note: Processing Algorithms," NCAR Research Aviation Facility, Boulder, 2019.
- [11] A. Cooper, A. Bailey and J. Carnes, "On Measuring Sensible-Heat Flux With Airborne Thermometers," NCAR RAF, Bounder, CO, 2021, preliminary copy.
- [12] W. Cooper, S. Spuler, M. Spowart, D. Lenschow and R. Friesen, "Calibrating Airborne Measurements of Airspeed, Pressure, and Temperature using a Doppler Laser Air-Motion Sensor," *Atmospheric Measurement Techniques*, vol. 7, pp. 3215-3231, 2014.